Scientific Research Publishing

Open Journal of Geology, 2024, 14, 760-786
https://www.scirp.org/journal/ojg
ISSN Online: 2161-7589
ISSN Print: 2161-7570

Magma Mixing Genesis of the Mafic Enclaves and Related Granitoids in the Kan Granite-Gneiss Complex of Central Côte d'Ivoire: Evidence from Geology, Petrology and Geochemistry

Koffi Raoul Teha[1*], Koffi Kossonou Jean-Marie Pria[2], Koffi Joseph Brou[1], Alain Nicaise Kouamelan[1], Marc Ephrem Allialy[1], Souad M'Rabet[3]

[1]Mineral and Energy Resources Laboratory (LGRME), Félix Houphouët-Boigny University, Abidjan, Ivory Coast
[2]Environmental Sciences and Technology Laboratory, Department of Earth Sciences, Jean Lorougnon-Guede Daloa University, Daloa, Ivory Coast
[3]Laboratory of Geosciences and Environment, Department of Geology, Ibn Tofaïl University of Kénitra, Kénitra, Morocco

Email: *rkteha@hotmail.fr

How to cite this paper: Teha, K.R., Pria, K.K.J.-M., Brou, K.J., Kouamelan, A.N., Allialy, M.E. and M'Rabet, S. (2024) Magma Mixing Genesis of the Mafic Enclaves and Related Granitoids in the Kan Granite-Gneiss Complex of Central Côte d'Ivoire: Evidence from Geology, Petrology and Geochemistry. *Open Journal of Geology*, **14**, 760-786.
https://doi.org/10.4236/ojg.2024.148033

Received: July 11, 2024
Accepted: August 23, 2024
Published: August 26, 2024

Abstract

The mafic enclaves from Paleoproterozoic domain are considered to be the results of large-scale crust-mantle interaction and magma mixing. In this paper, petrography, mineralogy and geochemistry were jointly used to determine the origin of the mafic enclaves and their relationship with the host granitoids of the Kan granite-gneiss complex. This study also provides new information on crust-mantle interactions. The mafic enclaves of the Kan vary in shape and size and have intermediate chemical compositions. The diagrams used show a number of similarities in the major elements (and often in the trace elements) between the mafic enclaves and the host granitoids. Geochemical show that the Kan rock are metaluminous, enriched in silica, medium to high-K calc-alkaline I-type granite. The similarities reflect a mixing of basic and acid magma. Mafic enclaves have a typical magmatic structure, which is characterized by magma mixing. The genesis of these rocks is associated with the context of subduction. They result from the mixing of a mafic magma originating from the mantle and linked to subduction, and a granitic magma (type I granite) that arises from the partial melting of the crust.

Keywords

Magma Mixing, Mafic Microgranular Enclaves, Host Granitoids, Kan

Granite-Gneiss Complex, West Africa

1. Introduction

The concept of two magmas mixing was first mentioned in the 1850s [1]. This is a process that occurs when two chemically distinct magmas mix to form a hybrid magma. Mafic microgranular enclaves (MME), schlierens, minerals out of equilibrium in their host rock, bedded rocks and hybrid rocks are the main observations that attest to magma mixing [2]. These characteristic features of magma mixing are observed in intermediate and felsic calc-alkaline granitoids [3]-[8].

The first (mafic microgranular enclaves) show (i) preliminary evidence of mantle heterogeneity and (ii) the role of mafic magmas in the initiation and evolution of calc-alkaline granitoid magmas [3] [9]. Mafic microgranular enclaves are excellent choices for interpreting the history of calc-alkaline pluton genesis. The enclaves also reflect incomplete mixing, a low proportion of injected basic material and poor representation in the plutonic rock [10]. According to the work of [3] [4] [11]-[14], the disintegration of dykes in host magmas influenced by the rheology of the materials involved is also at the origin of enclaves.

Schlierens represent the second case of magmatic mixing. They are important structures for deciphering the geological history of a region. They provide valuable insights into mineral crystallization conditions and the processes underlying rock formation and their chemical composition. Schlierens can have several origins and differ from enclaves in their elongation intensity [2]. However, some schlierens originate from enclave stretching [15]. Schlierens are found in the plutonic rocks described by [3] [15] [16].

Minerals formed during the cooling of magma are sometimes sensitive to physical and chemical conditions [17] [18]. The association of quartz and olivine minerals is impossible without invoking magmatic mixing. This is why [19] support the case of magmatic mixing between rhyolite and basalt to justify the presence of quartz and olivine in dacites. The bedded rocks correspond to the juxtaposition of different magmas during reservoir recharge. Hybrid rocks are rocks in which the initial constituents are no longer identifiable [2].

In this paper, the evidence of magmatic mixing that will be studied are the mafic microgranular enclaves. These enclaves, which vary in shape and size, outcrop in the granitoids of the Kan complex. The aim is to establish the field relationships, mineralogical composition and geochemical interaction of the mafic microgranular enclaves with the Kan granite-gneiss complex. Geochemical analysis will help to identify the geotectonic environment of the Kan complex.

2. Geological Background

2.1. West African Craton

The West African craton is made up of the Reguibat Rise and the Man-Leo Rise

(Figure 1(a)). These two rises are separated by the Taoudéni Basin (Figure 1(a)). The studied area is located within the Man-Leo Rise.

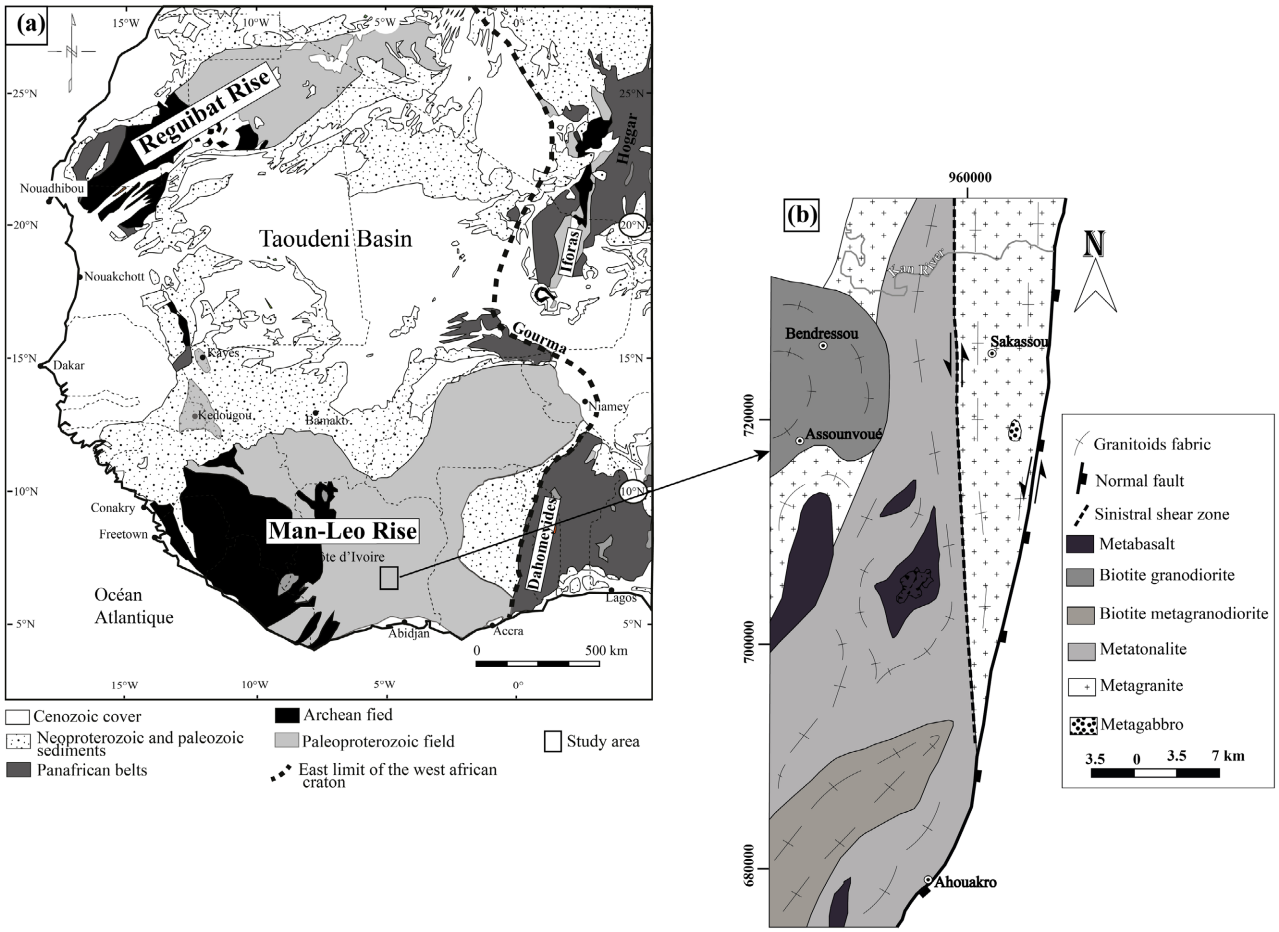

Figure 1. Geological maps. (a) Simplified geological map of the West African craton [34]. (b) Geological map of Kan granite-gneiss complex (modified after [29]).

The rocks comprising the Man-Leo Rise have undergone a complex geological history. The Man-Leo Rise is subdivided into two domains separated by the Sassandra shear zone. The Kénéma-Man domain located in the western part of the rise is essentially composed of Archean rocks including migmatites, gneisses, granulites and charnockites [20]-[23]. These rocks are dated between 3.2 Ga and 2.75 Ga [20]-[22]. The eastern part of the Man-Léo Ridge is occupied by the Paleoproterozoic domain. It is characterized by tholeiitic and calc-alkaline volcanics, granitoids, vocano-sediments and sediments. These rocks were emplaced between 2.25 and 2.05 Ga [24]-[26].

2.2. Kan Granite-Gneiss Complex

The geological history of the Kan granite-gneiss complex is intertwined with that of the West African craton (Figure 1(b)). The Kan granitoids were first defined by [27]. In this part of the Birimian domain, the author distinguishes three ma-

jor groups composed of the Kan River Group, the volcanic group and S-type intrusive granitoids [27] [28]. The Kan complex consists of amphibolite-facies TTG, mylonitic orthogneiss, mafic-ultramafic rocks and mylonitic gneiss [6] [27] [28]. These rocks are affected by intense ductile deformation. The Kan granitoids formed after the belts of Birimian rocks [29]. The volcanic group includes clastic metavolcanites, rare lavas and volcanosediments. It lies unconformably on the Kan rocks. The western part is occupied by the Comoé basin [29] [30]. The Kan complex and the Comoé basin are separated by the Dimbokro shear corridor [28]. In recent works, the granitoids of the Kan complex are interpreted to originate from juvenile crustal growth within a Paleoproterozoic orogen at the boundary of a convergent plate [31].

3. Field Observations of Mafic Enclaves

The Kan granite-gneiss complex contains several mafic microgranular enclaves of varying sizes, shapes and lengths (**Figure 2**). The mafic enclaves used in this

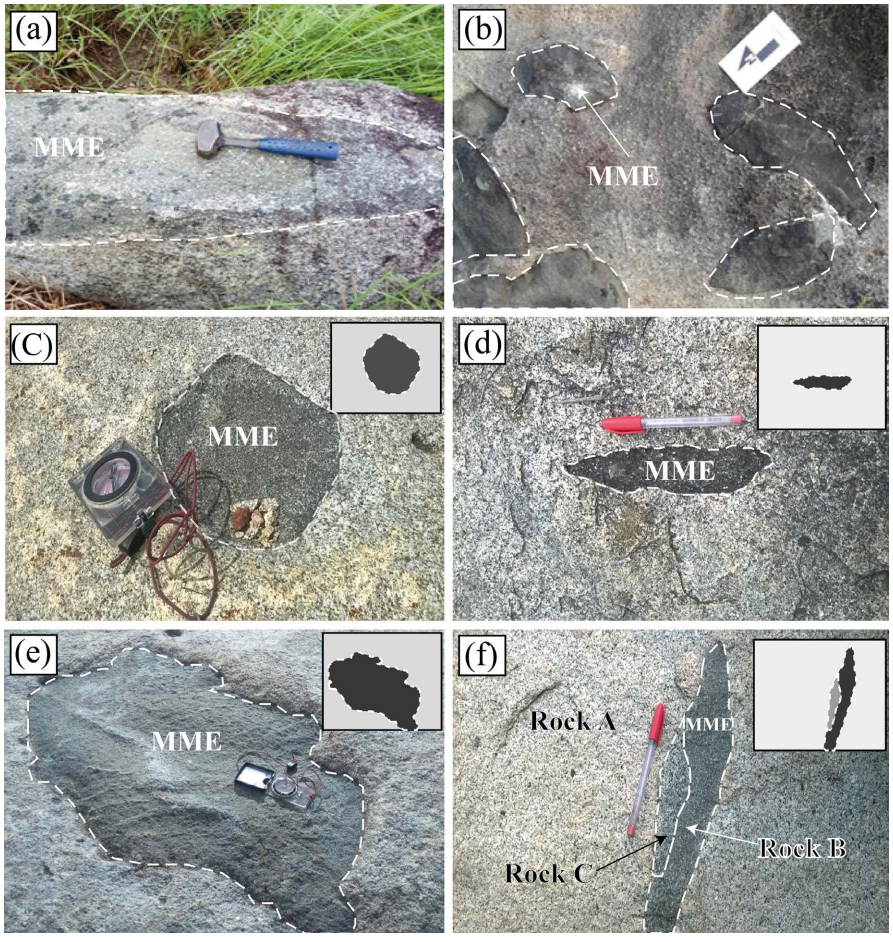

Figure 2. Different shapes and sizes of mafic microgranular enclaves. (a) Feldspar and amphibole phenocrysts in the enclave; (b) Cluster of mafic enclaves of varying shapes; (c) Sub-circular mafic magmatic enclave in a host granitoid; (d) Elongated mafic enclave; (e) Ovoid-shaped mafic enclave; (f) Different relationships between mafic enclaves. The enclaves show a sharp contact with the host granitoids.

study come from the localities of Ahouakro, Assounvoué, Bendressou and Sakassou (**Figure 1(b)**). As their name suggests, these are dark rocks with fine-grained microgranular textures. However, some enclaves show phenocrysts of feldspars and amphiboles derived from the host granitoids, suggesting the intermingling of several magmas (**Figure 2(a)**). The enclaves encountered are sometimes grouped in a single location and take several forms (**Figure 2(b)**). They range in size from centimetres to decimetres (**Figure 2**). The enclaves observed have sub-rounded to rounded shapes (**Figure 2(c)**). Rounded shapes correspond to partial assimilation in the magma [32]. Others are elongated, forming spheroids (**Figure 2(d)**). The most common are ovoid (**Figure 2(e)**). Several stages in the creation of enclaves have been identified. In some outcrops, for example, a rock contains an enclave of rock B which in turn contains an enclave of rock C (**Figure 2(f)**). The multitude of enclaves present reflect the frequency of interactions between different magmas. The contacts between the different enclaves may be rounded or angular. These contacts are generally very sharp with no evidence of deformation.

4. Analytical Methods

4.1. Mineral Chemistry

The chemical composition of amphibole and biotite minerals in the mafic microgranular enclaves was determined using a CAMECA SX 100 microprobe at the IFREMER laboratory in Brest (France). The operating conditions are 15 kV for the voltage and 20 mA for the intensity. Spot analyses were carried out on four thin sections that were initially metallized. Biotite and amphibole standards are used in the analytical procedure for Si, Al, Fe, Mg, Ti, Cl and F. Calibration was done according to [33].

4.2. Geochemistry

To determine the state of the chemical composition, analyses were performed by the BUREAU VERITAS laboratory in Vancouver, Canada. These analyses were conducted on eight fresh rocks, including four samples of mafic enclaves and four samples of host granitoids. The concentration of major oxides was determined using X-Ray fluorescence (XRF) spectrometry. Trace element concentrations were analyzed using inductively coupled plasma-mass spectrometry (ICP-MS). **Table 1** summarizes the major and trace element data for the analyzed samples.

5. Results

5.1. Samples Description

Microscopic observations reveal that the mafic enclaves sampled from different localities exhibit nearly similar mineralogical assemblages. The mineralogy is composed of amphibole, biotite, plagioclase, quartz and accessory minerals

Table 1. Major (wt%), trace and rare earth element (ppm) analyses of mafic magmatic enclaves and granitoids hosts in Kan granite-gneiss complex.

Samples Localities	MMEs				Granitoid hosts			
	TM21B Ahouakro	P50-2 Sakassou	P13-2 Assounvoué	P29-2 Bendressou	TM21A Ahouakro	P50-1 Sakassou	P13-1 Assounvoué	P29-1 Bendressou
Major elements (in wt.%)								
SiO_2	64.5	63.4	53.5	54.7	70.7	70.8	68.4	62.4
Al_2O_3	14.2	15.2	14.7	17.1	15.2	15.3	15.5	16.8
Fe_2O_3	6.08	6.43	9.03	8.91	2.62	2.4	3.71	5.66
CaO	4.4	3.7	8.27	7.11	2.47	2.68	3.05	5.12
MgO	3.66	3.16	5.52	4.37	0.9	1.07	1.17	2.54
Na_2O	4.55	4.04	3.04	4.11	4.71	5.09	4.45	4.52
K_2O	1.43	2.4	3.34	1.7	2.7	2.02	2.85	1.76
MnO	0.13	0.16	0.15	0.13	0.04	0.04	0.06	0.1
TiO_2	0.44	0.74	0.74	0.91	0.24	0.3	0.45	0.6
P_2O_5	0.13	0.24	0.24	0.32	0.07	0.09	0.16	0.22
Cr_2O_3	0.04	0.02	0.03	0.01	0.01	0.02	0.01	0.02
LOI	0.5	0.97	0.95	0.9	0.04	0.18	0.13	0.8
A/CNK	0.83	0.95	0.62	0.79	1.00	0.99	0.97	0.90
A/NK	1.57	1.64	1.71	1.99	1.42	1.45	1.49	1.80
Total	100.06	100.46	99.84	100.27	99.69	99.99	99.94	100.54
Trace elements (in ppm)								
Zr	109	99	176.3	136.6	97	96.6	148.8	136
Y	9.9	7.1	21.5	20.8	4.8	4.8	8.1	11.3
Mo	0.1	0.4	0.7	0.4	0.2	0.5	0.6	0.6
Cu	122	61.9	42	220.9	8.1	7.9	14.6	19.3
Pb	1.6	5.5	4.7	1.3	2.8	2.6	2.4	2.1
Zn	63	155	33	71	36	50	52	76
Ni	60.2	39.1	17.6	41.1	10.1	15	7.4	16.7
Cr	0.03	0.01	0.02	0.01	0.01	0.01	0.01	0.01
Th	2.4	3	3.7	1.6	5.3	2.1	6.7	4.1
U	2.4	2.8	1.4	1.1	1.1	0.7	1.3	1.4
V	80	119	215	176	29	28	58	98
Ta	0.3	0.7	0.4	0.3	0.3	0.3	0.6	0.6
Ba	334	365	2572	697	1212	848	1013	664
Be	3	4	4	3	2	1	2	1

Continued

Co	17.2	18.3	34.9	33.6	5.1	5.9	9.3	15.9
Cs	1.8	71.1	2.5	2.3	3.7	19.8	2.8	3.4
Ga	17.4	22.9	16.3	19.8	15.3	17.7	19.9	21.3
Hf	2.9	3	4.6	3.4	3	2.9	4	3.5
Nb	3.8	7.4	10.7	5.6	2.8	4.8	5.4	6.9
Rb	68	336.3	71.6	53.1	89	137.7	85.7	60.7
Sr	416.2	446.2	1211.7	764.2	507	615.7	659.4	798.8
La	13.6	9.1	34.4	25.9	10.2	13.8	30.4	24
Ce	25.1	20.5	74.8	60.3	24.3	29.1	58.4	50
Pr	2.87	2.51	9.34	8.2	2.16	3.13	5.99	6.04
Nd	11.2	10.6	37.9	35.8	7.7	12.9	21.7	24.3
Sm	2.33	2.28	8.08	6.8	1.36	2.21	3.51	4.25
Eu	0.56	0.79	2.3	1.73	0.46	0.64	1.01	1.29
Gd	2.01	2.07	7.26	5.33	1.16	1.82	2.64	3.26
Tb	0.3	0.29	0.95	0.71	0.16	0.21	0.31	0.4
Dy	1.55	1.49	4.59	3.77	0.87	0.96	1.45	2.26
Ho	0.32	0.3	0.84	0.74	0.14	0.17	0.25	0.41
Er	0.93	0.81	2.12	2.06	0.43	0.45	0.76	1.05
Tm	0.13	0.11	0.26	0.3	0.06	0.07	0.1	0.17
Yb	0.88	0.84	1.67	1.98	0.51	0.42	0.65	1.12
Lu	0.13	0.12	0.27	0.28	0.08	0.07	0.11	0.17
∑REE	61.91	51.81	184.78	153.9	49.59	65.95	127.28	118.72
Eu/Eu*	0.80	1.12	0.93	0.89	1.13	0.99	1.02	1.07
Ce/Ce*	0.94	1.01	0.98	0.97	1.22	1.04	1.02	0.98
La_N/Yb_N	10.20	7.15	13.60	8.64	13.21	21.70	30.88	14.15
La_N/Sm_N	3.56	2.43	2.60	2.32	4.57	3.81	5.28	3.44
Gd_N/Yb_N	1.83	1.98	3.49	2.16	1.83	3.48	3.26	2.34

(alteration mineral and oxides).

Amphibole is the predominant mineral found in the MMEs (**Figures 3(a)-(e)**). These amphiboles show variations in both shape and size (**Figures 3(a)-(c)**). They are green in color and display significant pleochroism. Amphibole is the main ferromagnesian mineral in MMEs. The amphiboles are mainly found alongside biotite and constitute around 40% of the minerals present in the rocks (**Figure 3(a)**, **Figure 3(b)**, **Figure 3(e)**). The amphibole crystals often form aggregates up to 6 mm in size (**Figure 3(b)**). They are often macerated, with frequent inclusions of biotite and oxides (**Figure 3(a)**). Some crystals show epidote alteration

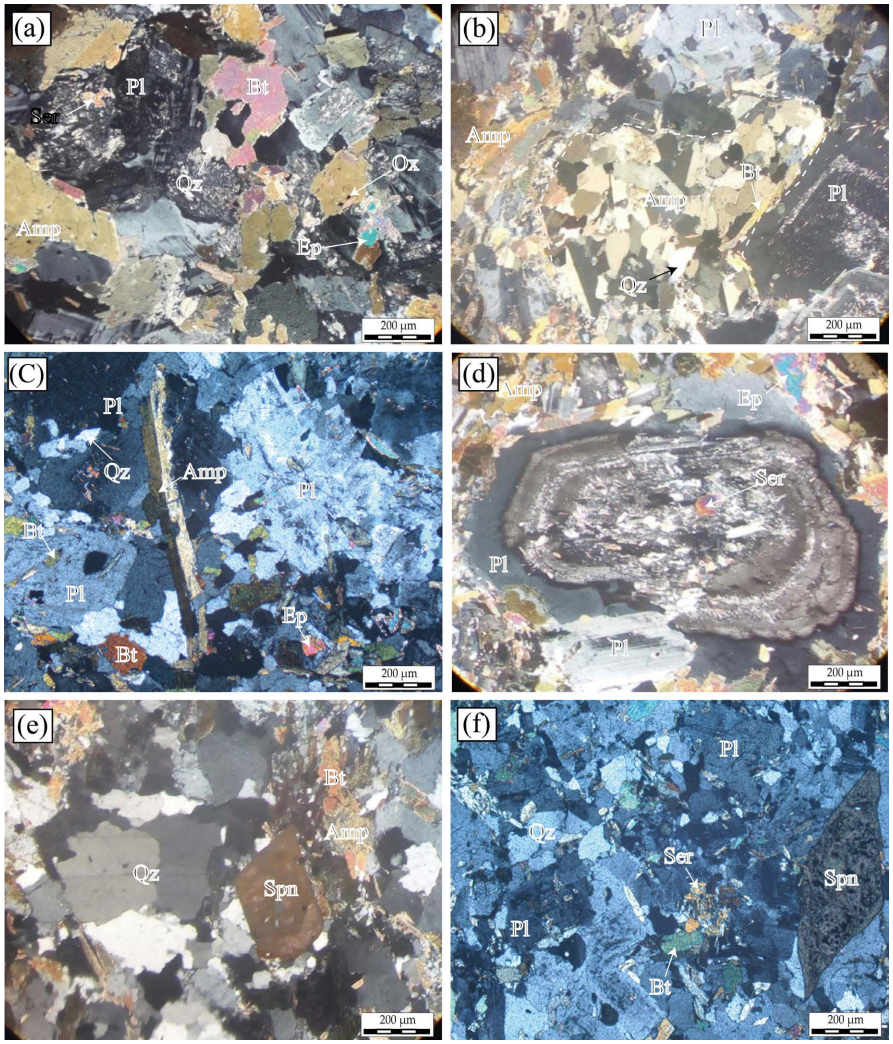

Figure 3. Representative photomicrographs of mafic microgranular enclaves. (a) Amphibole crystals of various shapes and sizes containing oxide inclusions and altered to epidote; (b) Amphibole aggregate and associated fine biotite band; (c) Elongated amphibole crystals; Plagioclase containing quartz and biotite inclusions; (d) Zoned plagioclase with core altered to sericite surrounded by amphibole often altered to epidote; (e) Clusters of quartz and sphene developing aureoles; (f) Oxide inclusions in sphene and alteration of plagioclase feldspars to sericite. Qz: Quartz; Spn: Sphene; Amp: Amphibole; Bt: Biotite; Ser: Sericite; Pl: Plagioclase; Ep: Epidote; Ox: Oxides.

(**Figure 3(a)**, **Figure 3(c)**, **Figure 3(d)**).

Biotite and amphibole form the ferromagnesian minerals of the mafic enclaves. They are frequently observed together in the thin sections. Biotite forms fine, medium-sized flakes in the microgranular matrix ((**Figure 3(b)**). It accounts for around 25% of the mineralogy. Inclusions of zircons and oxides are common in the biotite crystals.

Plagioclase crystals, which vary in size, account for an estimated 20% of the overall mineralogy. They frequently form subhedral phenocrysts up to 5 mm long with an average width of 2 mm (**Figures 3(a)-(d)**, **Figure 3(f)**). Plagioclases are zoned with sericite-altered cores (**Figure 3(d)**). Quartz and biotite inclusions

can also be observed (**Figure 3(c)**).

Quartz mineral makes up a relatively small proportion of the rock (around 10%). It forms small, clear crystals and occupies an interstitial position between plagioclase and ferromagnesian minerals (**Figures 3(a)-(c)**). Quartz crystals are often grouped in sub-rounded clusters (**Figure 3(e)**). Accessory minerals include epidote, sphene and zircon (**Figure 3(a)**, **Figures 3(d)-(f)**). Sphene develops large aureoles (**Figure 3(e)**) and oxide inclusions (**Figure 3(f)**).

5.2. Mineral Chemistry

5.2.1. Amphiboles

Amphiboles are one of the main halogen minerals capable of recording magmatic events [35] [36]. Microprobe analyses of amphiboles are given in **Table 2**. The amphiboles originate from mafic microgranular enclaves in the samples. They have intermediate contents of SiO_2 and low contents of TiO_2 and alkalis ($Na_2O + K_2O$). These contents are typical of amphiboles in subduction zones [35]-[38]. The Si content (Si in formula) makes it possible to distinguish magmatic amphiboles (Si between 5.1 - 7.4) from secondary amphiboles (Si between 7.4 - 8.1). These secondary amphiboles in the mafic enclaves could be the result of a change in the chemical composition of the magmatic amphiboles during the emplacement of the host granitoids [39]. The amphiboles were projected in the classification diagram of [40]. The diagrams show that the mafic enclaves are composed of amphiboles with values $(Na + K)_A \geq 0.5$ and $(Na + K)_A < 0.5$ (**Figure 4(a)** & **Figure 4(b)**). Thus, we distinguish edenites, magnesio-hornblendes and actinolites with a wide range in the magnesio-hornblendes domain. Amphiboles are rich in Mg and depleted in Fe with Mg/(Mg + Fe) ranging from 0.51 to 0.61. However, some amphibole crystals show a high Fe content, with Fe/(Fe + Mg) ratios of 0.51.

5.2.2. Biotites

Biotites can be used to estimate the conditions of genesis of the magmatic host rocks: oxygen fugacity of the parent magmas, liquidus temperature, typological classification of granitoids, and dating of the thermal events undergone by these rocks [41]. The results of microprobe analyses of biotites are given in **Table 3**. These results show high concentrations of MgO (12.00 wt.% - 13.71 wt.%), low concentrations of Al_2O_3 (14.92 wt.% - 16.25 wt.%) and FeO (16.48 wt.% - 18.45 wt.%). Mg/(Mg + Fe^{2+}) ratios of between 0.54 - 0.60 indicate that these are magnesio-biotites [42]. Using the MgO vs. Al_2O_3 diagram of [43], we can dissociate all the biotites according to their peraluminous, calc-alkaline or alkaline magmatic origin. Analysis of this diagram shows that the biotites in the mafic magmatic enclaves were generated by calc-alkaline magmatism (**Figure 4(c)**). The MgO-FeOt-Al_2O_3 ternary diagram uses biotites to distinguish igneous rocks crystallized from A, C or P magmas type [43]. Enclave biotites lie on the boundary between the realms of orogenic suites and S-type magmas (**Figure 4(d)**).

Table 2. Representative microphobe analyses of amphiboles from the Kan mafic microgranular enclaves.

Samples	Mafic enclaves																						
Spot	105	99	100	102	103	104	106	108	111	112	124	126	1	4	6	9	2	3	16	13	14	7	129	107
SiO_2	45.79	51.29	46.92	51.76	49.03	49.06	47.73	47.82	46.89	52.34	47.35	47.63	42.81	43.19	46.13	43.68	42.99	42.74	42.82	43.94	43.41	44.33	45.34	43.83
TiO_2	0.83	0.06	0.38	0.25	0.47	0.62	0.47	0.26	0.52	0.10	0.32	0.57	0.91	0.89	0.38	0.97	0.99	0.92	0.96	0.84	0.88	0.41	0.54	0.97
Al_2O_3	7.59	4.22	7.43	3.91	5.77	5.72	6.59	6.34	7.08	3.11	6.75	6.55	10.24	10.49	8.64	10.25	10.85	10.75	10.47	10.01	9.89	10.20	8.72	9.06
FeO	16.44	13.28	16.04	12.87	14.87	14.87	15.39	15.15	15.81	12.04	15.84	15.74	17.73	17.69	16.61	17.48	17.78	17.98	17.87	17.40	18.46	18.43	17.38	17.69
MnO	0.49	0.40	0.41	0.53	0.45	0.47	0.39	0.39	0.39	0.42	0.52	0.47	0.38	0.26	0.30	0.36	0.31	0.34	0.33	0.38	0.36	0.42	0.42	0.43
MgO	11.78	14.58	12.25	14.88	13.37	13.50	12.85	13.23	12.39	15.80	12.67	12.46	10.12	10.01	11.26	10.27	9.96	10.09	10.10	10.47	9.66	10.16	11.35	10.84
CaO	11.79	12.33	11.90	11.89	11.79	11.94	12.01	11.63	11.81	12.19	11.87	11.71	11.55	11.97	11.99	12.14	11.95	11.84	12.03	11.93	11.79	12.08	11.81	11.73
Na_2O	1.07	0.65	1.07	0.63	0.93	0.87	0.94	1.08	1.00	0.48	0.90	1.08	1.39	1.28	1.05	1.23	1.31	1.44	1.29	1.36	1.12	1.19	1.19	1.30
K_2O	0.80	0.30	0.69	0.32	0.52	0.51	0.63	0.54	0.76	0.19	0.68	0.68	1.17	1.15	0.79	1.22	1.29	1.21	1.20	1.12	1.11	1.04	0.84	0.96
Cr_2O_3	0.00	0.03	0.10	0.60	0.32	0.01	0.00	0.01	0.13	0.06	0.27	0.05	0.02	0.00	0.16	0.00	0.07	0.01	0.07	0.06	0.02	0.00	0.09	0.01
NiO	0.12	0.01	0.02	0.07	0.04	0.06	0.06	0.06	0.05	0.03	0.07	0.00	0.00	0.02	0.05	0.03	0.05	0.02	0.01	0.03	0.04	0.00	0.06	0.03
Total	96.73	97.16	97.25	97.70	97.56	97.63	97.04	96.51	96.83	96.79	97.24	96.95	96.31	96.95	97.36	97.63	97.55	97.35	97.15	97.52	96.73	98.26	97.76	96.88
Formula per 23 oxygens																								
Si in formula	6.91	7.49	7.01	7.51	7.23	7.23	7.11	7.15	7.03	7.62	7.07	7.12	6.57	6.58	6.91	6.60	6.52	6.51	6.53	6.64	6.64	6.66	6.80	6.68
^{IV}Al	1.08	0.50	0.99	0.49	0.77	0.77	0.89	0.85	0.97	0.38	0.93	0.88	1.43	1.42	1.09	1.40	1.48	1.49	1.47	1.36	1.35	1.33	1.19	1.32
^{VI}Al	0.27	0.22	0.32	0.18	0.23	0.22	0.27	0.27	0.28	0.15	0.26	0.27	0.43	0.46	0.43	0.43	0.46	0.43	0.41	0.42	0.43	0.47	0.35	0.31
Fe^{2+}	2.08	1.62	2.00	1.56	1.83	1.83	1.92	1.89	1.98	1.47	1.98	1.97	2.15	2.16	1.99	2.14	2.16	2.17	2.18	2.12	2.26	2.21	2.18	2.25
Mn^{2+}	0.06	0.05	0.05	0.07	0.06	0.06	0.05	0.05	0.05	0.05	0.07	0.06	0.00	0.00	0.00	0.00	0.00	0.00	0.00	0.00	0.00	0.00	0.05	0.06
Ca	1.91	1.93	1.90	1.85	1.86	1.88	1.92	1.86	1.90	1.90	1.90	1.87	1.90	1.95	1.92	1.97	1.94	1.93	1.97	1.93	1.93	1.94	1.90	1.91
Mg	2.65	3.17	2.73	3.22	2.94	2.97	2.85	2.95	2.77	3.43	2.82	2.77	2.32	2.27	2.51	2.31	2.25	2.29	2.30	2.36	2.20	2.28	2.54	2.46
Ni	0.01	0.00	0.00	0.01	0.00	0.01	0.01	0.01	0.01	0.00	0.01	0.00	0.00	0.00	0.00	0.00	0.00	0.00	0.00	0.00	0.00	0.00	0.01	0.00
Na	0.31	0.18	0.31	0.15	0.27	0.25	0.27	0.31	0.29	0.13	0.26	0.31	0.00	0.00	0.00	0.00	0.00	0.00	0.00	0.00	0.00	0.00	0.35	0.38
K	0.15	0.06	0.13	0.06	0.10	0.10	0.12	0.10	0.15	0.04	0.13	0.13	0.23	0.22	0.15	0.24	0.25	0.23	0.23	0.22	0.22	0.20	0.16	0.19
Ti	0.09	0.01	0.04	0.03	0.05	0.07	0.05	0.03	0.06	0.01	0.04	0.06	0.10	0.10	0.04	0.11	0.11	0.11	0.11	0.10	0.10	0.05	0.06	0.11
$(Na + K)_A$	0.47	0.24	0.44	0.21	0.36	0.34	0.39	0.42	0.44	0.17	0.39	0.44	0.23	0.22	0.15	0.24	0.25	0.23	0.23	0.22	0.22	0.20	0.51	0.57
Mg/(Mg + Fe)	0.56	0.66	0.58	0.67	0.62	0.62	0.60	0.61	0.58	0.70	0.59	0.59	0.00	0.00	0.00	0.00	0.00	0.00	0.00	0.00	0.00	0.00	0.54	0.52
Fe/(Fe + Mg)	0.44	0.34	0.42	0.33	0.38	0.38	0.40	0.39	0.42	0.30	0.41	0.41	0.48	0.49	0.44	0.48	0.49	0.49	0.49	0.47	0.51	0.49	0.46	0.48
Na + K + Ca	2.38	2.17	2.35	2.06	2.23	2.23	2.31	2.28	2.33	2.07	2.29	2.32	2.13	2.17	2.07	2.21	2.19	2.16	2.20	2.15	2.15	2.14	2.41	2.48

Structural formula based on 23 oxygen atoms.

Table 3. Representative electron-microphobe analyses of biotite from Kan mafic microgranular enclaves.

Samples	Mafic enclaves									
Spot	2	5	7	10	11	98	101	115	121	123
SiO_2	36.68	37.12	37.70	37.49	36.79	37.60	38.23	37.69	37.19	36.84
TiO_2	1.66	1.48	1.29	1.50	1.27	1.35	1.48	1.51	1.76	1.27
Al_2O_3	15.48	15.71	16.06	16.26	16.25	14.96	15.56	15.13	15.08	14.92
FeO	17.76	17.01	16.41	16.68	18.45	16.70	16.99	17.00	16.48	18.39
MnO	0.22	0.16	0.16	0.21	0.33	0.32	0.26	0.24	0.33	0.23
MgO	12.60	12.87	12.95	12.55	12.00	13.42	12.87	13.11	13.71	13.02
CaO	0.04	0.00	0.02	0.01	0.00	0.02	0.15	0.03	0.01	0.04
Na_2O	0.02	0.05	0.02	0.00	0.00	0.05	0.02	0.05	0.01	0.02
K_2O	10.08	9.82	10.16	10.13	9.54	9.50	8.98	9.53	9.16	9.20
Cr_2O_3	0.04	0.17	0.09	0.07	0.20	0.04	0.22	0.08	0.09	0.18
NiO	0.03	0.03	0.07	0.06	0.02	0.10	0.06	0.07	0.07	0.07
Total	94.61	94.42	94.93	94.96	94.85	94.05	94.84	94.45	93.89	94.18
Formula per 23 oxygens										
Si	5.62	5.66	5.70	5.67	5.61	5.74	5.76	5.73	5.67	5.66
^{IV}Al	2.38	2.34	2.30	2.33	2.39	2.26	2.24	2.27	2.33	2.34
^{VI}Al	0.41	0.48	0.56	0.57	0.54	0.43	0.52	0.44	0.38	0.36
Ti	0.19	0.17	0.15	0.17	0.15	0.15	0.17	0.17	0.20	0.15
Fe^{2+}	2.27	2.17	2.07	2.11	2.35	2.13	2.14	2.16	2.10	2.36
Mn^{2+}	0.03	0.02	0.02	0.03	0.04	0.04	0.03	0.03	0.04	0.03
Na	0.01	0.02	0.00	0.00	0.00	0.01	0.01	0.02	0.00	0.01
K	1.97	1.91	1.96	1.95	1.86	1.85	1.73	1.85	1.78	1.80
Mg	2.88	2.92	2.92	2.83	2.73	3.05	2.89	2.97	3.12	2.98
Cr	0.01	0.03	0.01	0.01	0.02	0.01	0.02	0.01	0.02	0.01
Ni	0.01	0.01	0.01	0.01	0.01	0.00	0.00	0.01	0.00	0.01
Ca	0.00	0.02	0.00	0.00	0.01	0.01	0.00	0.00	0.00	0.00
F	0.00	0.00	0.00	0.00	0.00	0.00	0.00	0.00	0.00	0.00
Cl	0.00	0.00	0.00	0.00	0.00	0.00	0.00	0.00	0.00	0.00
OHcalc	4.00	4.00	4.00	4.00	4.00	4.00	4.00	4.00	4.00	4.00
$Fe^{2+}/(Mg + Fe^{2+})$	0.44	0.43	0.41	0.43	0.46	0.41	0.43	0.42	0.40	0.44
$Mg/(Mg + Fe^{2+})$	0.56	0.57	0.59	0.57	0.54	0.59	0.57	0.58	0.60	0.56

Structural formula based on 23 oxygen atoms.

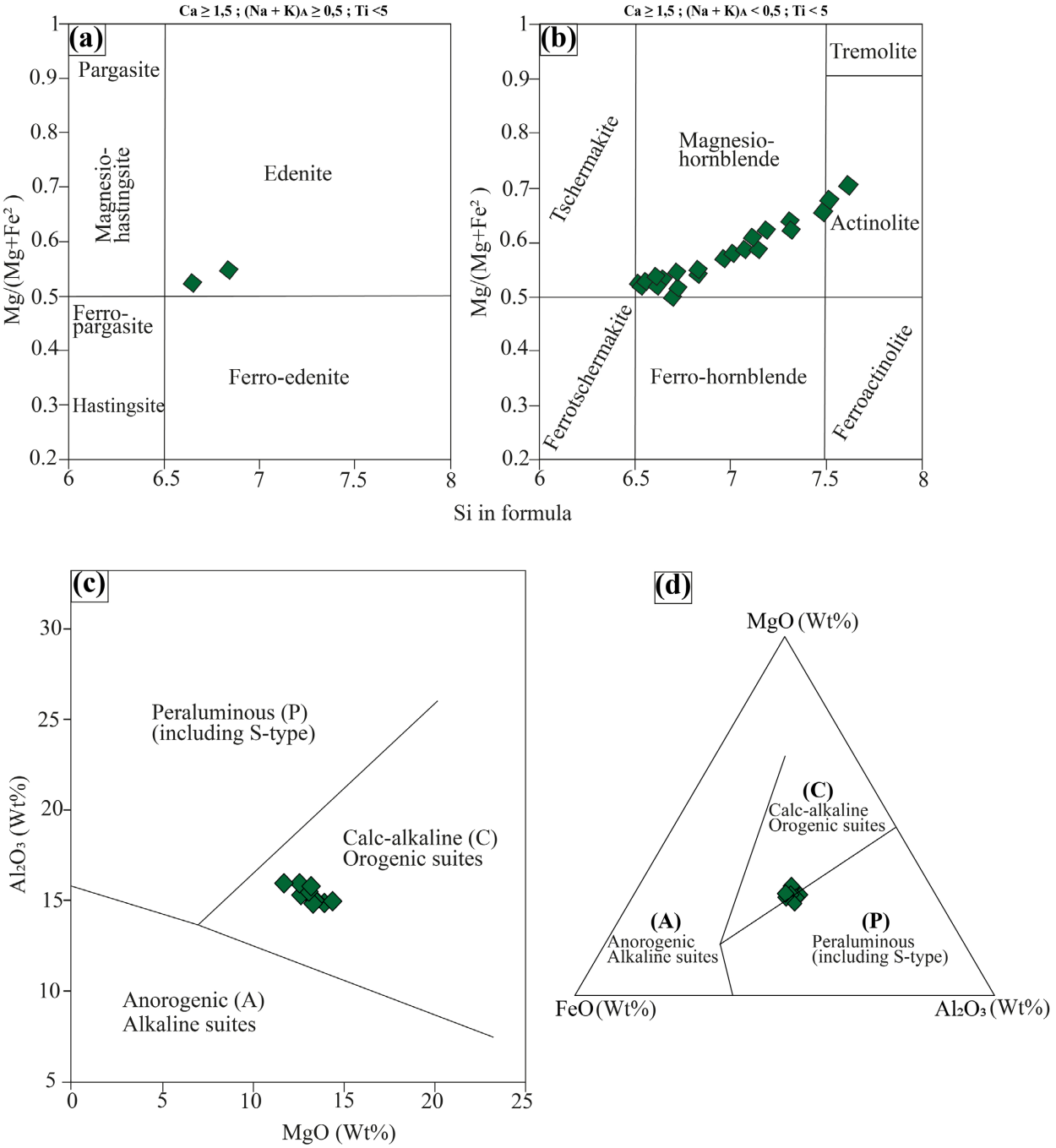

Figure 4. Diagrams discriminating amphiboles and biotites in the mafic microgranular enclaves. (a) Nomenclature of amphiboles from the study area in the Si vs. Mg/(Mg + Fe) diagram, with Na + K)$_A \geq 0.5$ [40]; (b) Nomenclature of amphiboles from the study area in the Si vs. Mg/(Mg + Fe) diagram, with (Na + K)$_A < 0.5$ [40]; (c) Discrimination of biotites in the MgO vs. Al_2O_3 diagram [43]; (d) Distribution of biotites in the MgO-FeOt-Al_2O_3 tectonomagmatic diagram [43].

5.3. Geochemistry Data

5.3.1. Major Element Geochemistry

The chemical compositions in SiO_2 vary from 53.5 wt.% to 64.5 wt.% for the mafic microgranular enclaves with an average of 59.06 wt.%. For the host granitoids, the SiO_2 composition ranges from 62.4 wt.% to 70.8 wt.% with an average

of 68.08 wt.% (Table 1). These compositions are intermediate and intermediate to felsic respectively. The MgO (3.16 wt.% - 5.52 wt.%), MnO (0.13 wt.% - 0.16 wt.%), TiO_2 (0.44 wt.%-0.91 wt.%) and P_2O_5 (0.13 wt.% - 0.32 wt.%) contents of the MMEs are higher than those observed in the Kan host granitoids where MgO ranges from 0.9 wt.% to 2.54 wt.%; MnO from 0.04 wt.% to 0.1 wt.%; TiO_2 from 0.24 wt.% to 0.6 wt.% and P_2O_5 from 0.07 wt.% to 0.22 wt.% (Table 1). The classification of the mafic enclaves investigated and their host rocks are shown in the SiO_2 (wt.%) vs. $Na_2O + K_2O$ (wt.%) diagram after [44]. According to this nomenclature, MMEs are composed of tonalite and monzodiorite (Figure 5(a)). The host granitoids range from tonalites to granodiorites and granites (Figure 5(a)).

The SiO_2 versus alkali-ratio diagram according to [45] shows that the microgranular mafic enclaves and their host granitoids have calc-alkaline affinities (Figure 5(b)). In detail, these rocks belong to the medium-K to high-K calc-alkaline series

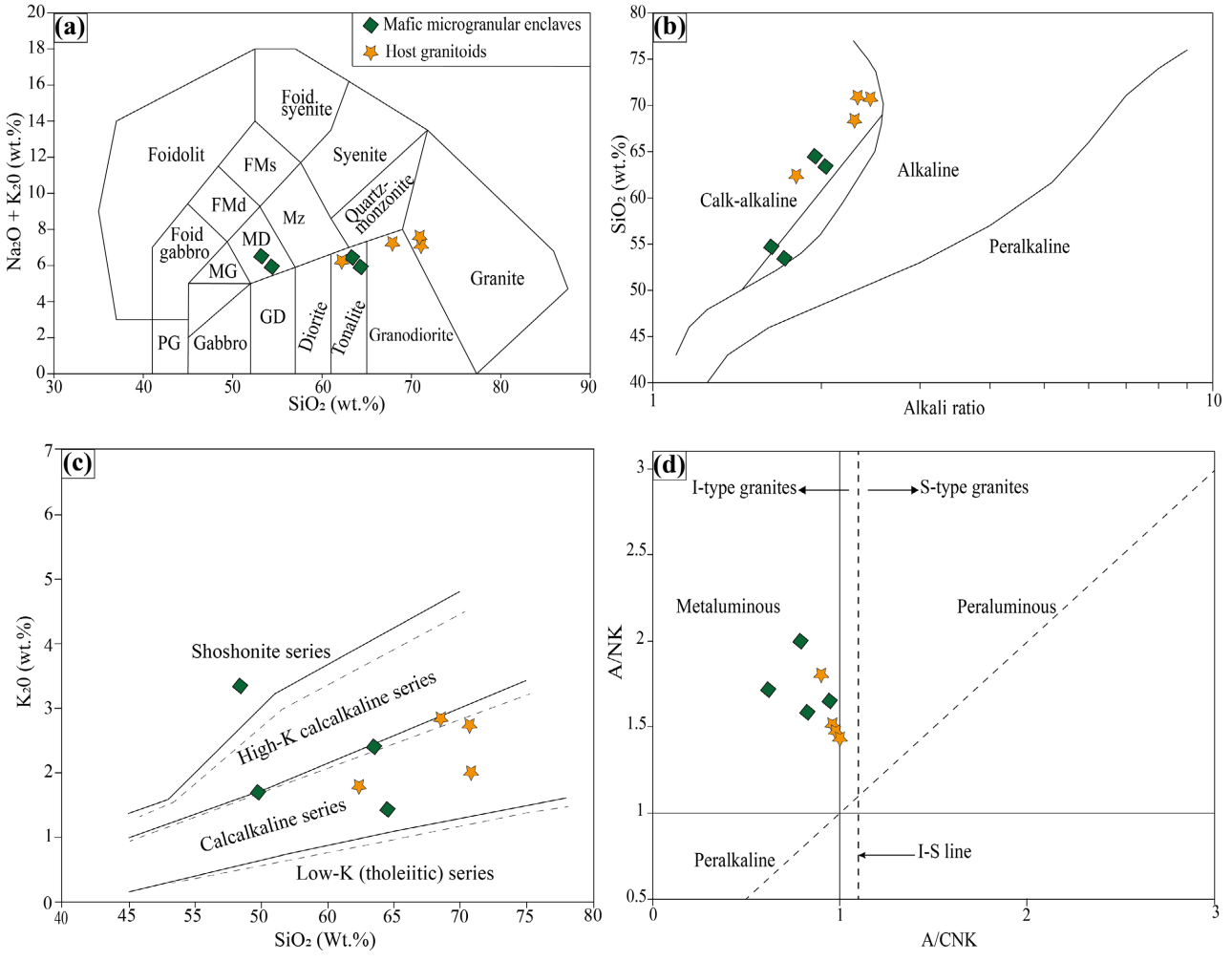

Figure 5. Chemical classification diagrams of the mafic enclaves and host granitoids of the Kan complex. (a) SiO_2 (wt.%) vs. $Na_2O + K_2O$ (wt.%) from [44]; (b) SiO_2 versus Alkali ratio diagram from [45]; (c) K_2O versus SiO_2 diagram with solid lines from [46] (dashed lines from [47]); (d) A/CNK vs. A/NK diagram from [48]. Abbreviations: FMs: Foid Monzosyenite; FMd: Foid Monzodiorite; Mz: Monzonite; MD: Monzodiorite; MG: Monzogabbro; GD: Gabbroic Diorite; PG: Peridotgabbro.

according to the diagram of [46] (**Figure 5(c)**). However, some enclaves show compositions that fall into the shoshonitic series (**Figure 5(c)**). K_2O contents vary from 1.43 wt.% to 3.34 wt.% for the MMEs and from 1.76 wt.% to 2.85 wt.% for the host granitoids (**Table 1**).

Al_2O_3 contents ranged from 14.20 wt.% to 17.10 wt.% for the MMEs with an average of 15.30 wt.% and from 15.20 wt.% to 16.80 wt.% for the host granitoids with an average of 15.70 wt.% (**Table 1**). The relatively low A/CNK values, ranging from 0.62 to 1.00, show that the MMEs and their hosts are metaluminous (**Table 1**, **Figure 5(d)**). This metaluminous character and the absence of peraluminous minerals (e.g. cordierite, sillimanite and andalusite) demonstrate that all the rocks studied are type-I granitoids (**Figure 5(d)**).

5.3.2. Trace Element Geochemistry

The rare earth and multi-element patterns can be seen in **Figure 6**. The former is the chondrites-normalized [49] and the latter is the primitive mantle-normalized [50]. Overall, the rare earth patterns all show a negative slope, with varying degrees of LREE/HREE fractionation. In detail, variations appear between the patterns of each petrographic entity.

The mafic microgranular enclaves and host granitoids show patterns moderately enriched in light rare earths with an average of 65.87 and 62.22 La_N respectively. In the mafic enclaves, the rare earths are slightly fractionated (La_N/Yb_N = 7.15 - 13.60) whereas the host granitoids show high La_N/Yb_N fractionation rates ranging from 13.21 - 30.88 (**Table 1**). The rare earth elements show comparatively similar and almost flat heavy rare earth profiles with an average Dy_N/Lu_N of

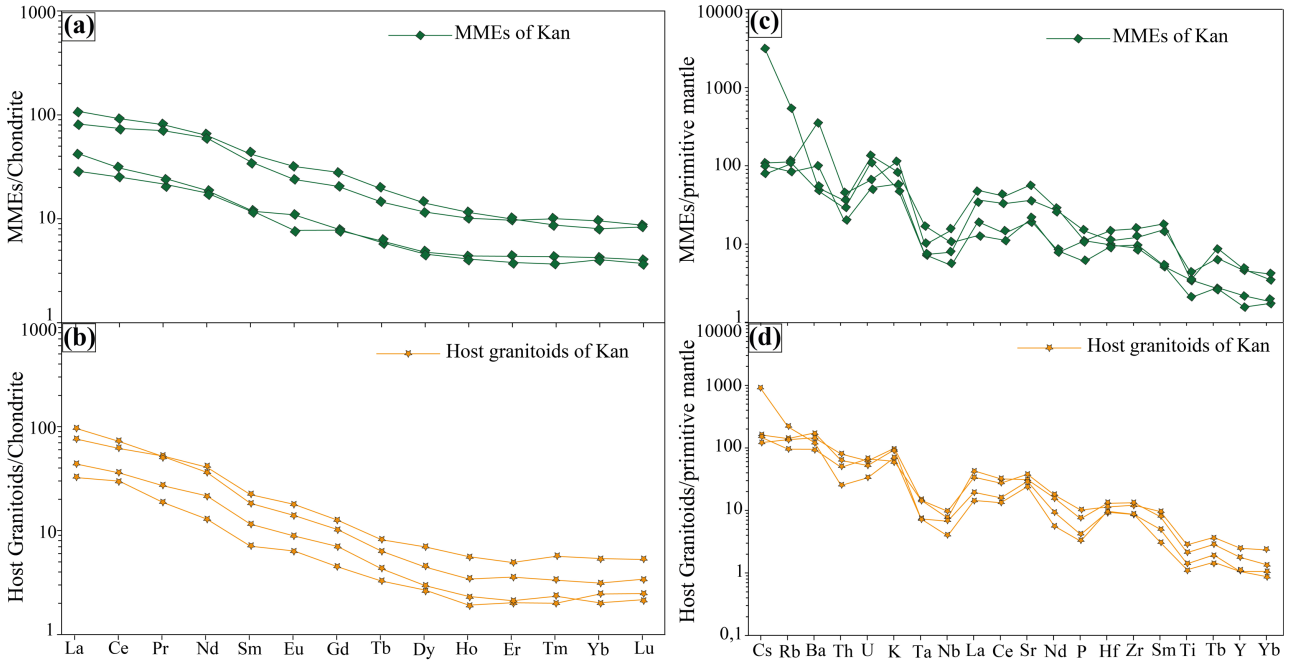

Figure 6. Chondrite-normalized REE patterns [49] of mafic microgranular enclaves (a) and hosts granitoids (b) and primitive mantle-normalized trace element patterns [50] of mafic microgranular enclaves (c) and hosts granitoids (d) of Kan complex.

1.36 for the mafic enclaves and 1.27 for the host granitoids (**Figure 6(a)**, **Figure 6(b)**). The MMEs (Eu/Eu*= 0.80 - 0.93) show profiles with negative Eu anomalies except for one mafic enclave sample which shows a positive Eu anomaly (Eu/Eu* = 1.12) (**Figure 6(a)**). In granitoids, rare earth patterns do not show negative anomalies (near zero). However, two samples of host granitoids show slight positive Eu anomalies (Eu/Eu* = 1.07 - 1.13) (**Figure 6(b)**). These positive anomalies suggest that the plagioclases did not fractionate during magmatic differentiation and that they are present in the form of cumulates [51] [52].

The primitive mantle-normalized trace element patterns (**Figure 6(c)**, **Figure 6(d)**) show that mafic microgranular enclaves and host granitoids are enriched in large ion lithophile elements (LILEs) such as Ba, K, Sr and La. MMEs and host rocks are depleted in high field strength elements (HFSEs) such as Nb, Ta, Ti and P (e.g. Late Triassic MMEs and granitoids, [53]). However, there are differences in the concentrations of trace elements. MMEs show higher concentrations of Ba up to 2572 ppm, Sr up to 1211.7 ppm, Cs up to 71.1 ppm, U compared to the host granitoids (**Table 1**, **Figure 6(c)**, **Figure 6(d)**). The mantle compatible elements (Co, Cu, Ni and Cr) have higher contents in the mafic enclaves than in the host granitoids (**Table 1**).

6. Discussion

6.1. Characteristics of Magma Mixing

The granitoids of the Kan complex are composed of abundant mafic microgranular enclaves, double enclave and plagioclase megacrysts visible in both MMEs and host granitoids. These field observations indicate the role played by magmatic mixing in the generation of these granitoids [3] [53]. Another fact illustrating magma mixing process in the Kan complex is the presence of sharp boundaries in the MMEs with their granitoid hosts. The variable shapes and sizes of MMEs could suggest variations in the viscosity of magmas, and MMEs and host granitoids have distinct parent magmas [54]-[58]. The mafic enclaves have a typical magmatic structure, which is characterized by magma mixing between high-temperature basic magma and low-temperature acidic magma through injecting [59].

Geochemically, similarities (alkaline, metaluminous and type I granite affinities) were observed between MMEs and host granitoids (**Figure 5**). [3] explains this similarity between MMEs and hosts as the result of diffusion and percolation processes. For [56], these similarities result from chemical exchange between mafic enclaves and rock hosts during re-equilibration. The use of biotite chemistry in the ternary diagram of [57] shows that the biotites in MMEs have undergone more or less complete chemical re-equilibration by a late-magmatic hydrothermal fluid (**Figure 7**). Bi-element SiO_2 versus Oxides Harker diagrams show a continuous and linear distribution of points representative of MMEs and granitoid host samples (**Figure 8**). This distribution indicates negative correlations between SiO_2 and Al_2O_3, Fe_2O_3, CaO, MgO, MnO and TiO_2. There is a

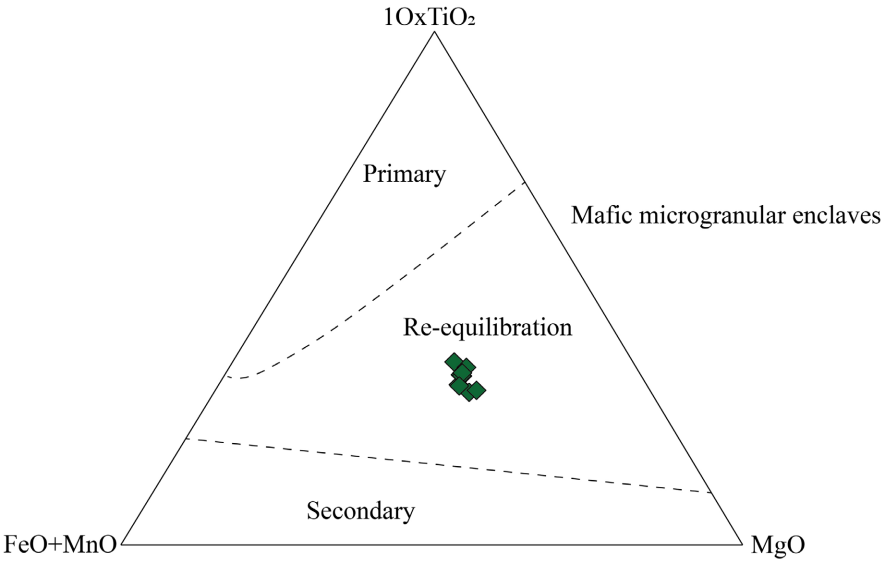

Figure 7. Disposition of biotites in mafic microgranular enclaves in the diagram of [57].

positive correlation between SiO_2 and Na_2O, but this is less clear-cut with K_2O, which appears to be negative. The approximately linear distribution of MMEs and host granitoids suggests a magma mixing phenomenon between acidic and basic magmas [58]-[62].

However, huge variations, reflecting magma mixing, are observed when MMEs and hosts are studied in detail. Harker diagrams also show that MMEs are enriched in Fe_2O_3, CaO, MgO, MnO, K_2O and TiO_2 compared to the host granitoids (**Figure 8**). Conversely, alkali (Na_2O) content in host granitoids is higher than in MMEs (**Figure 8**). The Al_2O_3/CaO vs. Na_2O/CaO and K_2O/CaO vs. SiO_2/CaO diagrams show linear trends of representative points of host MMEs and granitoids (**Figure 9(a)**, **Figure 9(b)**). Hyperbolic mixing arrays can be observed in the CaO/Al_2O_3 vs. K_2O/MgO plot (**Figure 9(c)**). These two trends reflect the occurrence of magma mixing (e.g. [38] [53] [59]). In the MgO vs. FeOt diagram by [62], the major oxide content shows a distribution along the hybridization trend (**Figure 9(d)**).

Finally, the similarities observed in the chondrite-normalized REE patterns (LREE/HREE enrichment), confirmed in the primitive mantle-normalized patterns, imply a certain homogenization between MMEs and hosts in the trace elements during magma mixing [63] (**Figure 6**).

6.2. Petrogenesis and Magma Sources

The linear distribution of MMEs and host granitoids in Harker diagrams also reflects fractional crystallization processes [64] [65] (**Figure 8**). Furthermore, the transition elements P_2O_5, TiO_2 and Cr_2O_3 each account for less than 1% in the mafic microgranular enclaves and host granitoid and there is a negative correlation between TiO_2 and SiO_2. This is due to the effect of fractional crystallization processes from the start of magma formation with the early genesis of rutile,

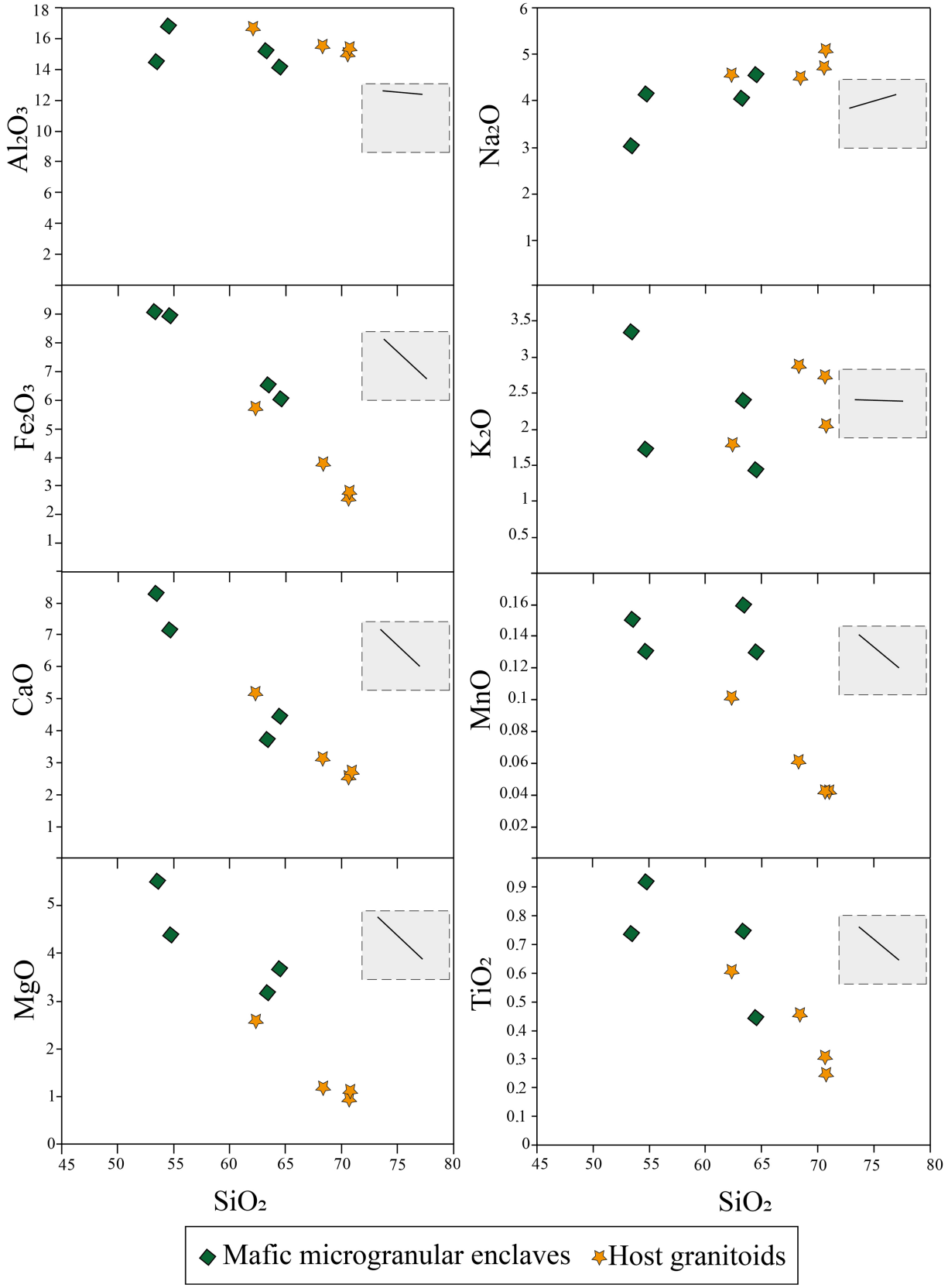

Figure 8. Distribution of MMEs and host granitoids in Harker diagrams. The inserts with solid lines show the trend in host rocks and mafic enclaves.

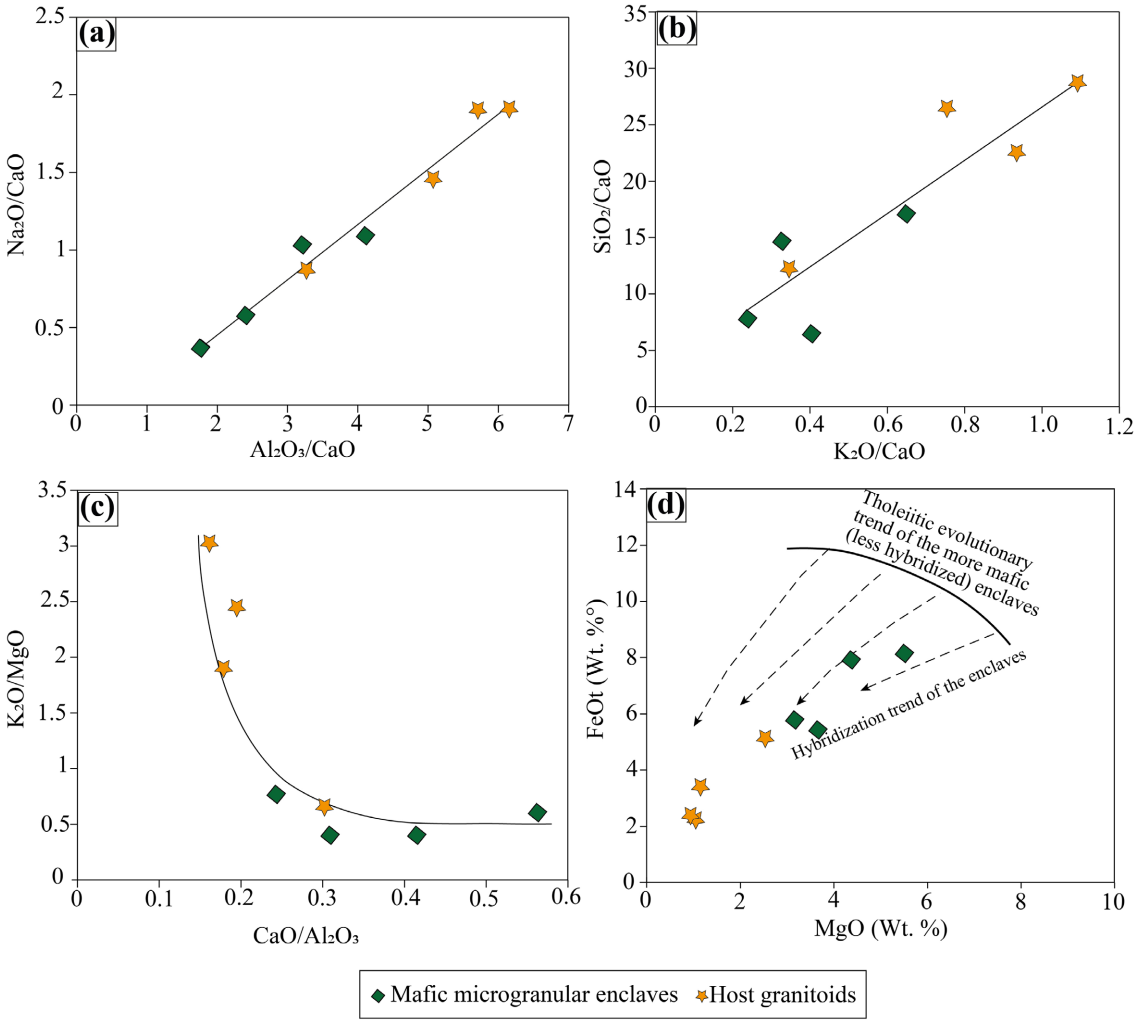

Figure 9. Geochemical correlation diagrams for mafic microgranular enclaves and host granitoids. (d) after [62].

ilmenite and apatite minerals [66]. The low Eu and Ti anamoly reflect the crystallization of plagioclase and sphene minerals respectively. The significant negative Nb anomalies indicate the role played by titaniferous and amphibole phases [67]. The presence of hornblende explains the low Yb content of magmas [68] [69].

In magmatic differentiation where fractional crystallization is the only process, the points representing trace elements follow a curve [70]. The Rb vs. Sr and Ba vs. Sr spaces show a large dispersion of the trace element points (**Figure 10(a)**, **Figure 10(b)**). This dispersion demonstrates that the relationship between the different petrographic entities is not controlled exclusively by a crystallization differentiation process, but also by partial melting (Haïmeur et al., 2004). High La_N/Yb_N ratios (up to 30.88) reflect a higher partial melting rate in the rocks and a different source [71]. The MMEs and host granitoids are metaluminous with acid to intermediate signatures and belong to type-I granite (**Figure 5(d)**). Type-I granites have been generated by partial melting of mafic to intermediate crustal rocks [72]-[74].

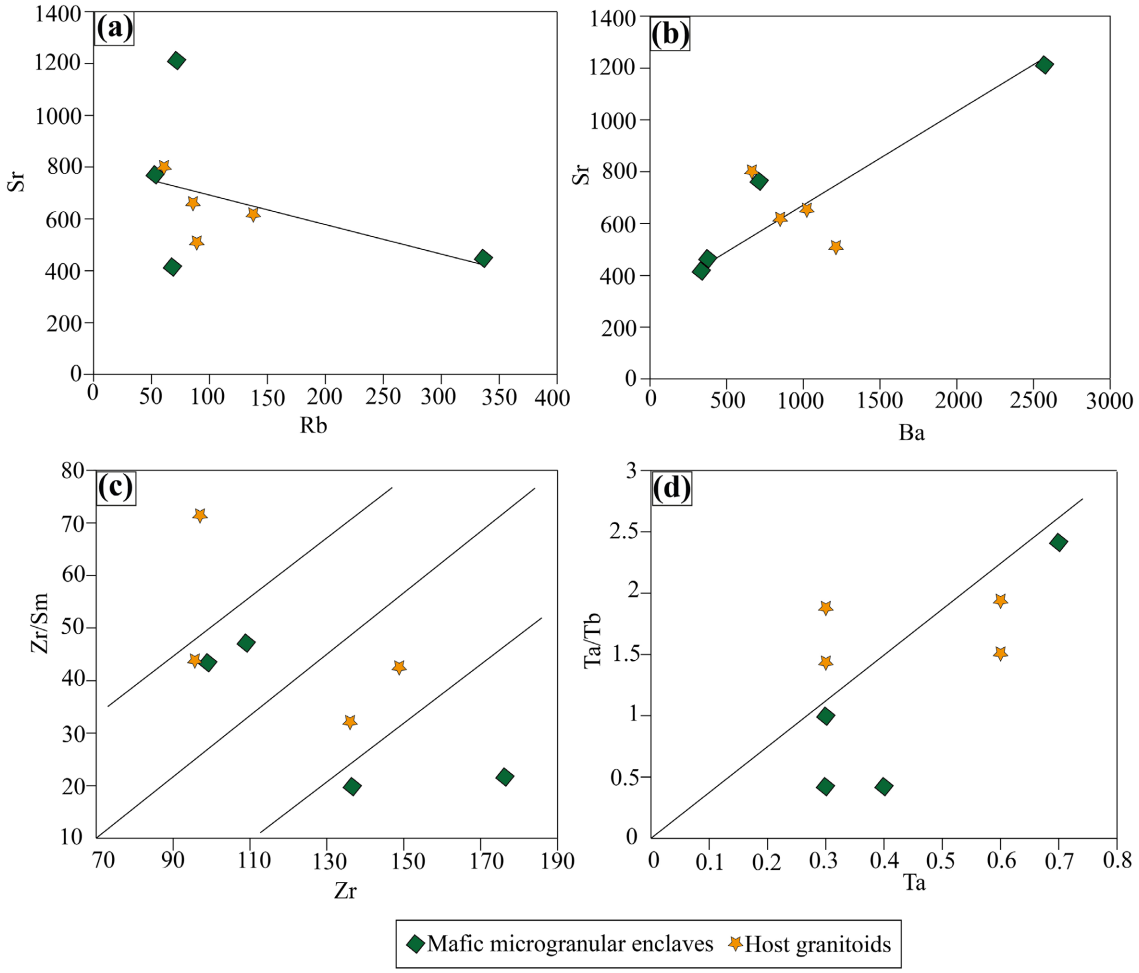

Figure 10. Plots of some pairs of trace elements. (a) Sr vs. Rb; (b) Sr vs (Ba); (c) Zr/Sm vs. Zr; (d) Ta/Tb vs. Ta.

Nb/Ta ratios range from 10.57 to 26.75 for mafic enclave samples and from 9 to 16 for host granitoids. The maximum value (26.75) is higher than that for basaltic oceanic crust, which is 17. The high field strength elements (Nb and Ta) are used in the genesis of magmas. The high ratios indicate that MMEs may represent the final basic element in the magma mixing [59]. MMEs and host granitoids show enrichment in LILEs and depletion in HFSEs, which implies that the ascent of mafic magmas was contaminated by continental crust [75].

Binary diagrams comparing the ratios of incompatible elements such as Zr vs. Zr/Sm and Ta vs. Ta/Tb can be used to investigate potential genetic relationships between magmas [76]. When the points representing the samples align along a straight line passing through the origin of the graphs, it indicates a partial melting process within the crust. Conversely, if the points align along straight lines parallel to those passing through the origin of the graphs, it reflects the evolution of magma originating from multiple sources and involving variable modalities of magma mixing or crustal contamination [77]. The analysis of the Zr vs. Zr/Sm diagram indicates that all the samples of enclaves and host granitoids are distributed almost entirely along two parallel lines that do not pass through the origin of the graph

(Figure 10(c)). This suggests that the different rocks have distinct parent magmas. These magmas result from the mixing of acid and basic magmas. The Ta vs. Ta/Tb diagram shows that partial melting processes underlie the crust and, to a lesser extent, confirm multiple sources and magma mixing (Figure 10(d)).

6.3. Tectonic Implication

The average Nb/Ta ratio is 17.16 (close to the primitive mantle, 17.5 ± 2, according to [78] for the MMEs and 11.45 for the host granitoids. The enclaves therefore reflect the contribution of the lithospheric mantle (e.g. [59]). The La/Yb vs. Nb/La diagram [79] confirms the lithospheric mantle origin of the mafic enclaves, far from the average lower crust (unlike the host granitoids, average lower crust La/Yb = 30.26 and Nb/La = 0.27; Figure 11(a)). However, the MMEs field extends into the mixed lithospheric-asthenospheric mantle domain (Figure 11(a)).

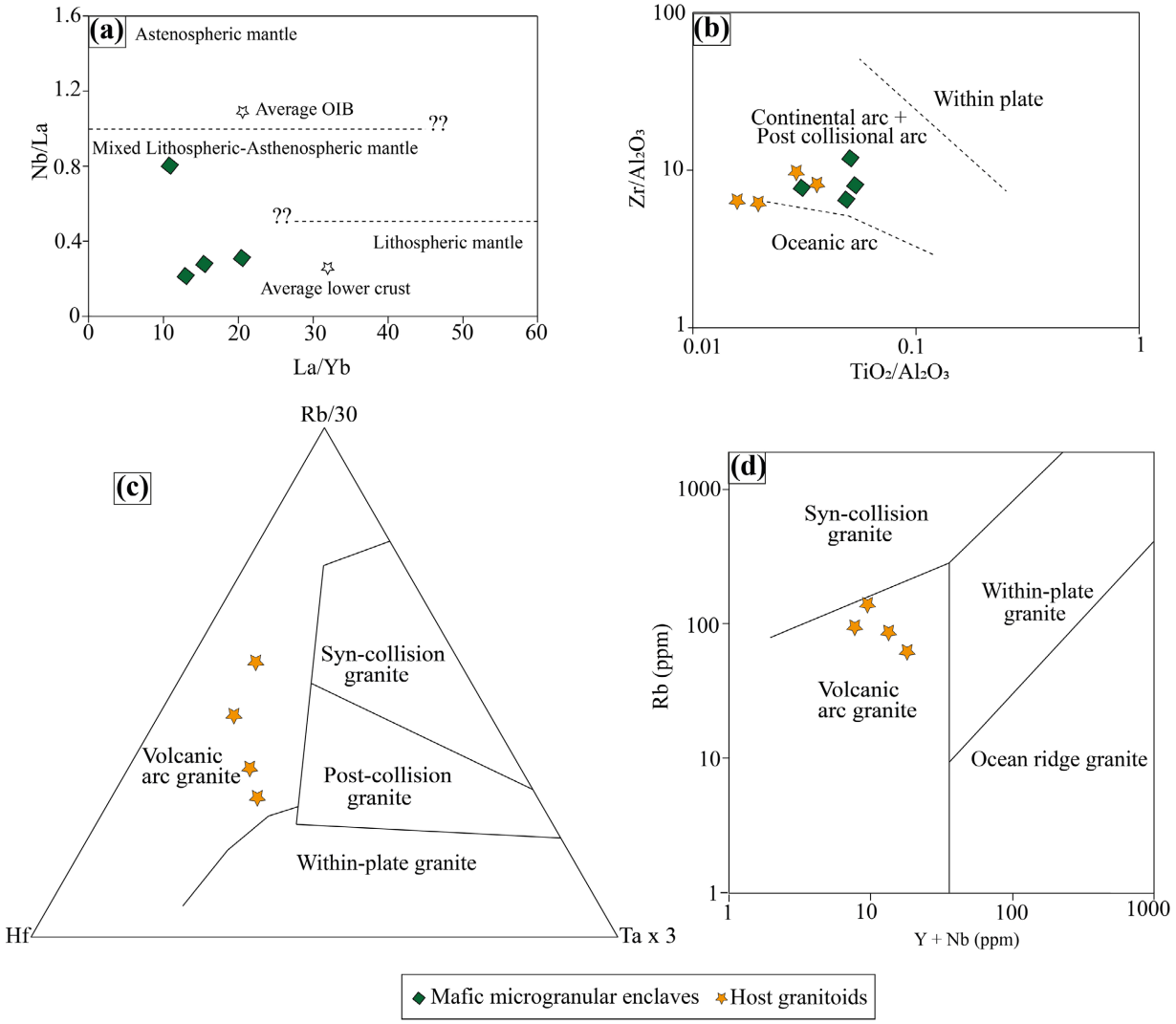

Figure 11. Tectonic discrimination diagrams for MMEs and host granitoids. (a) La/Yb vs. Nb/La diagram to distinguish of the lithospheric and asthenospheric mantle (after [79]); (b) TiO_2/Al_2O_3 vs. Zr/Al_2O_3 diagram for mafic microgranular enclaves and host granitoïds (after [82]); (c) Rb/30-Ta x 3-Hf diagram (after [83]); (d) Y + Nb vs. Rb diagram [84].

The primitive mantle-normalized patterns highlight negative anomalies of Nb, Ta and Ti which are typical of magmas from subduction zones [80] [81]. This subduction zone environment is reflected in the TiO_2/Al_2O_3 vs. Zr/Al_2O_3 diagram [82] where mafic enclaves and host granitoids fall within the field of continental arcs and at the boundary of oceanic arcs (**Figure 11(b)**). It results from the convergence of an oceanic lithospheric plate and a continental lithospheric plate. Furthermore, the host granitoids were inserted into the Rb/30-Ta x 3-Hf and Y+Nb vs. Rb tectonic discrimination diagrams according to [83] and [84] respectively (**Figure 11(c)**, **Figure 11(d)**). Due to their low Ta, Y and Nb contents, all the host granitoids fall within the fields of volcanic arc granites (VAG), thus confirming the subduction environment. The absence of Eu anomalies in some host granitoids is thought to be due to the melting of a hydrated subducted oceanic crust. This occurred within a moderately deep subduction zone that reacted with the mantle wedge at the base of the adjacent continental crust. Under such conditions, no Eu anomalies are expected to appear [67].

7. Conclusions

In this paper, the evidence of magma mixing lies in the presence of the mafic microgranular enclaves. A combination of field data, petrographic and chemical (minerals and whole-rocks) methods demonstrate the mixing of two magmas.

1) Field and petrographic data consisting of mafic enclaves provide evidence of magma mixing. This evidence includes enclaves of various shapes and sizes, sharp contact surfaces between the host and the enclaves, and the presence of phenocrysts of feldspars belonging to the host granitoids found in the mafic enclaves.

2) Chemically, the MMEs studied are composed of tonalites and monzodiorite with intermediate compositions. The host granitoids are composed of granite, granodiorite and tonalite with intermediate to acid compositions. Although embedded in granites, granodiorite, tonalite and highly mafic, the MMEs show almost similar chemical affinities (alkaline, metaluminous, type I granite) to their hosts.

3) Host mafic enclaves and granitoids result from the mixing of basic and acid magmas. They were formed by processes dominated by partial melting of the lithospheric mantle and granitic magma derived from the continental crust in a subduction context.

Further work will focus on zircon U-Pb dating to prove that the host rocks and mafic enclaves were emplaced at the same time.

Acknowledgements

This work is the result of thesis work by T.K.R. and P.K.K.J.-M. It received financial support from the T2GEM project (Geophysical and Geochemical Technologies for Mining Exploration). We would like to thank Kouamé Junior for his involvement in the production of this paper.

Conflicts of Interest

The authors declare no conflicts of interest regarding the publication of this paper.

References

[1] Bunsen, R. (1851) Ueber die Processe der vulkanischen Gesteinsbildungen Islands. *Annalen der Physik*, **159**, 197-272. https://doi.org/10.1002/andp.18511590602

[2] Laumonier, M. (2013) Mélange de magmas à HP-HT, contraintes expérimentales et application au magmatisme d'arc. Master's Thesis, Université d'Orléans,.

[3] Barbarin, B. (2005) Mafic Magmatic Enclaves and Mafic Rocks Associated with Some Granitoids of the Central Sierra Nevada Batholith, California: Nature, Origin, and Relations with the Hosts. *Lithos*, **80**, 155-177. https://doi.org/10.1016/j.lithos.2004.05.010

[4] Barbarin, B. and Didier, J. (1992) Genesis and Evolution of Mafic Microgranular Enclaves through Various Types of Interaction between Coexisting Felsic and Mafic Magmas. *Earth and Environmental Science Transactions of the Royal Society of Edinburgh*, **83**, 145-153.

[5] Jafari, A., Fazlnia, A. and Jamei, S. (2014) Mafic Enclaves in North of Urumieh Plutonic Complex: Evidence of Magma Mixing and Mingling, Sanandaj-Sirjan Zone, NW Iran. *Arabian Journal of Geosciences*, **8**, 7191-7206. https://doi.org/10.1007/s12517-014-1701-7

[6] Pria, K.K.J.M. (2021) Caractéristiques pétrographique, structurale et géochimique du complexe granito-gneissique du kan (région est de Toumodi, centre de la côte d'ivoire): Implication dans la géodynamique des formations Paléoprotérozoïque du craton ouest-africain. Master's Thesis, Université Félix Houphouët-Boigny.

[7] Ramiz, M.M. and Mondal, M.E.A. (2016) Petrogenesis of Mafic Magmatic Enclaves of the Bundelkhand Granitoids near Orchha, Central Indian Shield: Evidence for Rapid Crystallization. *Geological Society, London, Special Publications*, **449**, 159-173. https://doi.org/10.1144/sp449.6

[8] Teha, K.R. (2019) Les formations éburnéennes du sud-ouest du bassin de la Comoé et du secteur de Singrobo (Sud de la Côte d'Ivoire): Pétrologie, analyse structurale et magmatisme associé. Master's Thesis, Université Félix Houphouët-Boigny.

[9] Tedonkenfack, S.S.T., Tamen, J., Nkouathio, D.G., Asaah, A.N.E., Gountié-Dedzoedzo, M. and Aka, F.T. (2019) Petrography and Geochemistry of Mantle Xenoliths from Ibal-Oku Region (North-West Region, Cameroon): Preliminary Evidence of Mantle Heterogeneities. *Journal of African Earth Sciences*, **154**, 70-79. https://doi.org/10.1016/j.jafrearsci.2019.03.019

[10] Barbarin, B. (1990) Granitoids: Main Petrogenetic Classifications in Relation to Origin and Tectonic Setting. *Geological Journal*, **25**, 227-238. https://doi.org/10.1002/gj.3350250306

[11] Castro, A., de la Rosa, J.D. and Stephens, W.E. (1990) Magma Mixing in the Subvolcanic Environment: Petrology of the Gerena Interaction Zone near Seville, Spain. *Contributions to Mineralogy and Petrology*, **106**, 9-26. https://doi.org/10.1007/bf00306405

[12] Fernandez, A.N. and Gasquet, D.R. (1994) Relative Rheological Evolution of Chemically Contrasted Coeval Magmas: Example of the Tichka Plutonic Complex (Morocco). *Contributions to Mineralogy and Petrology*, **116**, 316-326. https://doi.org/10.1007/bf00306500

[13] Pons, J., Barbey, P., Nachit, H. and Burg, J.P. (2006) Development of Igneous Layering during Growth of Pluton: The Tarçouate Laccolith (Morocco). *Tectonophysics*, **413**, 271-286. https://doi.org/10.1016/j.tecto.2005.11.005

[14] Turnbull, R., Weaver, S., Tulloch, A., Cole, J., Handler, M. and Ireland, T. (2010) Field and Geochemical Constraints on Mafic-Felsic Interactions, and Processes in High-Level Arc Magma Chambers: An Example from the Halfmoon Pluton, New Zealand. *Journal of Petrology*, **51**, 1477-1505. https://doi.org/10.1093/petrology/egq026

[15] Barbey, P., Gasquet, D., Pin, C. and Bourgeix, A.L. (2008) Igneous Banding, Schlieren and Mafic Enclaves in Calc-Alkaline Granites: The Budduso Pluton (Sardinia). *Lithos*, **104**, 147-163. https://doi.org/10.1016/j.lithos.2007.12.004

[16] Asrat, A., Barbey, P., Ludden, J.N., Reisberg, L., Gleizes, G. and Ayalew, D. (2004) Petrology and Isotope Geochemistry of the Pan-African Negash Pluton, Northern Ethiopia: Mafic-Felsic Magma Interactions during the Construction of Shallow-Level Calc-Alkaline Plutons. *Journal of Petrology*, **45**, 1147-1179. https://doi.org/10.1093/petrology/egh009

[17] Davì, M., De Rosa, R. and Holtz, F. (2010) Mafic Enclaves in the Rhyolitic Products of Lipari Historical Eruptions; Relationships with the Coeval Vulcano Magmas (aeolian Islands, Italy). *Bulletin of Volcanology*, **72**, 991-1008. https://doi.org/10.1007/s00445-010-0376-5

[18] Guan, Q., Zhu, D., Zhao, Z., Dong, G., Zhang, L., Li, X., *et al.* (2012) Crustal Thickening Prior to 38 Ma in Southern Tibet: Evidence from Lower Crust-Derived Adakitic Magmatism in the Gangdese Batholith. *Gondwana Research*, **21**, 88-99. https://doi.org/10.1016/j.gr.2011.07.004

[19] Pal, T., Mitra, S.K., Sengupta, S., Katari, A., Bandopadhyay, P.C. and Bhattacharya, A.K. (2007) Dacite-Andesites of Narcondam Volcano in the Andaman Sea—An Imprint of Magma Mixing in the Inner Arc of the Andaman-Java Subduction System. *Journal of Volcanology and Geothermal Research*, **168**, 93-113. https://doi.org/10.1016/j.jvolgeores.2007.08.005

[20] Gouedji, F., Picard, C., Coulibaly, Y., Audet, M., Auge, T., Goncalves, P., *et al.* (2014) The Samapleu Mafic-Ultramafic Intrusion and Its Ni-Cu-PGE Mineralization: An Eburnean (2.09 Ga) Feeder Dyke to the Yacouba Layered Complex (Man Archean Craton, Western Ivory Coast). *Bulletin de la Société Géologique de France*, **185**, 393-411. https://doi.org/10.2113/gssgfbull.185.6.393

[21] Koffi, G.R., Kouamelan, A.N., Allialy, M.E., Coulibaly, Y. and Peucat, J. (2020) Re-Evaluation of Leonian and Liberian Events in the Geodynamical Evolution of the Man-Leo Shield (West African Craton). *Precambrian Research*, **338**, Article ID: 105582. https://doi.org/10.1016/j.precamres.2019.105582

[22] Kouamelan, A.N., Delor, C. and Peucat, J. (1997) Geochronological Evidence for Reworking of Archean Terrains during the Early Proterozoic (2.1 Ga) in the Western Côte D'ivoire (Man Rise-West African Craton). *Precambrian Research*, **86**, 177-199. https://doi.org/10.1016/s0301-9268(97)00043-0

[23] Wright, J.B., Hastings, D.A., Jones, W.B. and Williams, H.R. (1985) Geology and Mineral Resources of West Africa. Springer.

[24] Baratoux, L., Metelka, V., Naba, S., Jessell, M.W., Grégoire, M. and Ganne, J. (2011) Juvenile Paleoproterozoic Crust Evolution during the Eburnean Orogeny (~2.2-2.0ga), Western Burkina Faso. *Precambrian Research*, **191**, 18-45. https://doi.org/10.1016/j.precamres.2011.08.010

[25] Doumbia, S., Pouclet, A., Kouamelan, A., Peucat, J.J., Vidal, M. and Delor, C. (1998) Petrogenesis of Juvenile-Type Birimian (Paleoproterozoic) Granitoids in Central Côte-

d'Ivoire, West Africa: Geochemistry and Geochronology. *Precambrian Research*, **87**, 33-63. https://doi.org/10.1016/s0301-9268(97)00201-5

[26] Pouclet, A., Vidal, M., Delor, C., Simeon, Y., Alric, G. (1996). Le volcanisme birimien du nordest de la Côte d'Ivoire, mise en évidence de deux phases volcano-tectoniques distinctes dans l'évolution géodynamique du Paléoprotérozoïque. *Bulletin de la Société Géologique de France*, **167**, 529-541.

[27] Mortimer, J. (1990). Evolution of the Early Proterozoic Toumodi Volcanic Group and Associated Rocks, Ivory Coast. Portsmouth Polytechnic, 244 p.

[28] Mortimer, J. (1992) The Kan River Gneiss Terrane of Central Côte D'ivoire: Mylonitic Remnants of an Ancient Magmatic Arc? *Journal of African Earth Sciences* (*and the Middle East*), **15**, 353-367. https://doi.org/10.1016/0899-5362(92)90020-d

[29] Delor, C., Daouda, Y.B., Simeon, Y., Diaby, I., Gadou, G., Kohou, P., Konan, G., Dom-maget, A. and Tastet, J.P. (1992) Carte géologique de la Côte d'ivoire à 1/200 000, feuille d'Abidjan Ministère des Mines et de l'Energie. Direction de la Géologie, Abidjan, Côte d'ivoire.

[30] Vidal, M., Delor, C., Pouclet, A., Simeon, Y., Alric, G. (1996). Evolution géodynamique de l'Afrique de l'Ouest entre 2,2 Ga et 2 Ga: Le style archéen des ceintures vertes et des ensembles sédimentaires birimiens du nordest de la Côte-d'Ivoire. *Bulletin de la Société géologique de France*, **167**, 307-319.

[31] Mortimer, J. (2016) Paleoproterozoic Geology of the Toumodi Area, Ivory Coast, 1:100,000. *Journal of Maps*, **12**, 392-400. https://doi.org/10.1080/17445647.2016.1227732

[32] Ramsay, J.G. (1989) Emplacement Kinematics of a Granite Diapir: The Chindamora Batholith, Zimbabwe. *Journal of Structural Geology*, **11**, 191-209. https://doi.org/10.1016/0191-8141(89)90043-6

[33] Popp, R.K., Virgo, D., Yoder, H.S., Hoering, T.C. and Phillips, M.W. (1995) An Experimental Study of Phase Equilibria and Fe Oxy-Component in Kaersutitic Amphibole; Implications for the f_{h2} and a_{H2O} in the Upper Mantle. *American Mineralogist*, **80**, 534-548. https://doi.org/10.2138/am-1995-5-613

[34] Béziat, D., Bourges, F., Debat, P., Lompo, M., Martin, F. and Tollon, F. (2000) A Paleoproterozoic Ultramafic-Mafic Assemblage and Associated Volcanic Rocks of the Boromo Greenstone Belt: Fractionates Originating from Island-Arc Volcanic Activity in the West African Craton. *Precambrian Research*, **101**, 25-47. https://doi.org/10.1016/s0301-9268(99)00085-6

[35] Manthilake, G., Koga, K.T., Peng, Y. and Mookherjee, M. (2021) Halogen Bearing Amphiboles, Aqueous Fluids, and Melts in Subduction Zones: Insights on Halogen Cycle from Electrical Conductivity. *Journal of Geophysical Research*: *Solid Earth*, **126**, e2020JB021339. https://doi.org/10.1029/2020jb021339

[36] Martin, R.F. (2007) Amphiboles in the Igneous Environment. *Reviews in Mineralogy and Geochemistry*, **67**, 323-358. https://doi.org/10.2138/rmg.2007.67.9

[37] Coltorti, M., Bonadiman, C., Faccini, B., Grégoire, M., O'Reilly, S.Y. and Powell, W. (2007) Amphiboles from Suprasubduction and Intraplate Lithospheric Mantle. *Lithos*, **99**, 68-84. https://doi.org/10.1016/j.lithos.2007.05.009

[38] Liu, L., Qiu, J. and Li, Z. (2013) Origin of Mafic Microgranular Enclaves (MMEs) and Their Host Quartz Monzonites from the Muchen Pluton in Zhejiang Province, Southeast China: Implications for Magma Mixing and Crust-Mantle Interaction. *Lithos*, **160**, 145-163. https://doi.org/10.1016/j.lithos.2012.12.005

[39] Leake, B.E. (1971) On Aluminous and Edenitic Hornblendes. *Mineralogical Magazine*, **38**, 389-407. https://doi.org/10.1180/minmag.1971.038.296.01

[40] Leake, B.E., Woolley, A.R., Arps, C.E.S., Birch, W.D., Gilbert, M.C., Grice, J.D., *et al.* (1997) Nomenclature of Amphiboles Report of the Subcommittee on Amphiboles of the International Mineralogical Association Commission on New Minerals and Mineral Names. *European Journal of Mineralogy*, **9**, 623-651. https://doi.org/10.1127/ejm/9/3/0623

[41] Nachit, H., Ibhi, A., Abia, E.H. and Ben Ohoud, M. (2005) Discrimination between Primary Magmatic Biotites, Reequilibrated Biotites and Neoformed Biotites. *Comptes Rendus. Géoscience*, **337**, 1415-1420. https://doi.org/10.1016/j.crte.2005.09.002

[42] Foster, M.D. (1960) Interpretation of the Composition of Trioctahedral Micas. Geological Survey Professional Paper 354-B 49.

[43] Abdel-Rahman, A.M. (1994) Nature of Biotites from Alkaline, Calc-Alkaline, and Peraluminous Magmas. *Journal of Petrology*, **35**, 525-541. https://doi.org/10.1093/petrology/35.2.525

[44] Middlemost, E.A.K. (1994) Naming Materials in the Magma/Igneous Rock System. *Earth-Science Reviews*, **37**, 215-224. https://doi.org/10.1016/0012-8252(94)90029-9

[45] Wright, J.B. (1969) A Simple Alkalinity Ratio and Its Application to Questions of Non-Orogenic Granite Genesis. *Geological Magazine*, **106**, 370-384. https://doi.org/10.1017/s0016756800058222

[46] Peccerillo, A. and Taylor, S.R. (1976) Geochemistry of Eocene Calc-Alkaline Volcanic Rocks from the Kastamonu Area, Northern Turkey. *Contributions to Mineralogy and Petrology*, **58**, 63-81. https://doi.org/10.1007/bf00384745

[47] T. J. B. H. (1986) E. A. K. Middlemost 1985. Magmas and Magmatic Rocks. an Introduction to Igneous Petrology. X + 266 Pp. London, New York: Longman. Price £13.95 (paperback). ISBN 0 582 30080 0. *Geological Magazine*, **123**, 87-88. https://doi.org/10.1017/s0016756800026716

[48] Maniar, P.D. and Piccoli, P.M. (1989) Tectonic Discrimination of Granitoids. *Geological Society of America Bulletin*, **101**, 635-643. https://doi.org/10.1130/0016-7606(1989)101<0635:tdog>2.3.co;2

[49] McDonough, W.F. and Sun, S.-S. (1995) The Composition of the Earth. *Chemical Geology*, **120**, 223-253. https://doi.org/10.1016/0009-2541(94)00140-4

[50] Sun, S.S. and McDonough, W.F. (1989) Chemical and Isotopic Systematics of Oceanic Basalts: Implications for Mantle Composition and Processes. *Geological Society, London, Special Publications*, **42**, 313-345. https://doi.org/10.1144/gsl.sp.1989.042.01.19

[51] Haïmeur, J., El Amrani El Hassani, I.E. and Chabane, A. (2004) Pétrologie et géochimie des granitoïdes calco-alcalins de Zaër (Maroc central): Modèle pétrogénétique. *Bulletin de l'Institut Scientifique, Rabat, section Sciences de la Terre*, **26**, 27-48.

[52] Ramiz, M.M., Ahmad, I., Mondal, M.E.A. and Rahaman, W. (2022) Multistage Neoarchean Magma Genesis in the Bundelkhand Craton, India: Evidence from Whole-Rock Elemental and Nd Isotopic Study of Mafic Magmatic Enclaves and Granitoids. *Geosystems and Geoenvironment*, **1**, Article 100085. https://doi.org/10.1016/j.geogeo.2022.100085

[53] Xie, H., Wang, Y., Li, D., Zhou, G. and Zhang, Z. (2021) Late Triassic Magma Mixing and Fractional Crystallization in the Qingchengzi Orefield, Eastern Liaoning Province: Regional Petrogenetic and Metallogenic Implications. *Journal of Earth Science*, **32**, 144-157. https://doi.org/10.1007/s12583-020-1114-3

[54] Arvin, M., Dargahi, S. and Babaei, A.A. (2004) Mafic Microgranular Enclave Swarms in the Chenar Granitoid Stock, NW of Kerman, Iran: Evidence for Magma Mingling. *Journal of Asian Earth Sciences*, **24**, 105-113.

https://doi.org/10.1016/j.jseaes.2003.09.004

[55] Kumar, S., Rino, V. and Pal, A.B. (2004) Field Evidence of Magma Mixing from Microgranular Enclaves Hosted in Palaeoproterozoic Malanjkhand Granitoids, Central India. *Gondwana Research*, **7**, 539-548. https://doi.org/10.1016/s1342-937x(05)70804-2

[56] Dorais, M.J., Whitney, J.A. and Roden, M.F. (1990) Origin of Mafic Enclaves in the Dinkey Creek Pluton, Central Sierra Nevada Batholith, California. *Journal of Petrology*, **31**, 853-881. https://doi.org/10.1093/petrology/31.4.853

[57] Nachit, H., Razafimahefa, N., Stussi, J.M. and Carron, J.P. (1985) Composition chimique des biotites et typologie magmatique des granitoids. *Comptes Rendus Hebdoma-daires de l'Académie des Sciences*, **301**, 813-818.

[58] Clemens, J.D. and Wall, V.J. (1981) Origin and Crystallization of Some Peraluminous (S-Type) Granitic Magmas. *The Canadian Mineralogist*, **19**, 111-131.

[59] Huang, L., Wang, L., Fan, H., Lin, M. and Zhang, W. (2020) Late Early-Cretaceous Magma Mixing in the Langqi Island, Fujian Province, China: Evidences from Petrology, Geochemistry and Zircon Geochronology. *Journal of Earth Science*, **31**, 468-480. https://doi.org/10.1007/s12583-019-1022-7

[60] Kouchi, A. and Sunagawa, I. (1985) A Model for Mixing Basaltic and Dacitic Magmas as Deduced from Experimental Data. *Contributions to Mineralogy and Petrology*, **89**, 17-23. https://doi.org/10.1007/bf01177586

[61] Roman, D.C., Cashman, K.V., Gardner, C.A., Wallace, P.J. and Donovan, J.J. (2005) Storage and Interaction of Compositionally Heterogeneous Magmas from the 1986 Eruption of Augustine Volcano, Alaska. *Bulletin of Volcanology*, **68**, 240-254. https://doi.org/10.1007/s00445-005-0003-z

[62] Zorpi, M.J., Coulon, C., Orsini, J.B. and Cocirta, C. (1989) Magma Mingling, Zoning and Emplacement in Calc-Alkaline Granitoid Plutons. *Tectonophysics*, **157**, 315-329. https://doi.org/10.1016/0040-1951(89)90147-9

[63] Qin, J., Lai, S., Grapes, R., Diwu, C., Ju, Y. and Li, Y. (2009) Geochemical Evidence for Origin of Magma Mixing for the Triassic Monzonitic Granite and Its Enclaves at Mishuling in the Qinling Orogen (Central China). *Lithos*, **112**, 259-276. https://doi.org/10.1016/j.lithos.2009.03.007

[64] Orsini, J.B., Cocirta, C. and Zorpi, M.J. (1991) Genesis of Mafic Microgranular Enclaves trough Differenciation of Basic Magmas, Mingling and Chemical Exchanges with Their Host Granitoid Magmas. In: Didier, J. and Barbarin, B., Eds., *Enclaves and Granite Petrology*, Elsevier, 445-463.

[65] Boukaoud, E.H. (2007) Étude pétrographique et géochimique des pegmatites de Sidi Mezghiche (Wilaya de Skikda, nord-est algérien). Master's Thesis, Université Mentouri Constantine.

[66] Moyen, J., Martin, H. and Jayananda, M. (1997) Origine du granite fini-Archéen de Closepet (Inde du Sud): Apports de la modélisation géochimique du comportement des éléments en trace. *Comptes Rendus de l'Académie des Sciences—Series IIA—Earth and Planetary Science*, **325**, 659-664. https://doi.org/10.1016/s1251-8050(97)89107-0

[67] Martin, H. (1999) Adakitic Magmas: Modern Analogues of Archaean Granitoids. *Lithos*, **46**, 411-429. https://doi.org/10.1016/s0024-4937(98)00076-0

[68] Rogers, G. and Hawkesworth, C.J. (1989) A Geochemical Traverse across the North Chilean Andes: Evidence for Crust Generation from the Mantle Wedge. *Earth and Planetary Science Letters*, **91**, 271-285. https://doi.org/10.1016/0012-821x(89)90003-4

[69] Sigmarsson, O., Condomines, M., Morris, J.D. and Harmon, R.S. (1990) Uranium and 10be Enrichments by Fluids in Andean Arc Magmas. *Nature*, **346**, 163-165. https://doi.org/10.1038/346163a0

[70] Esna-Ashari, A., Valizadeh, M.V., Soltani, A. and Sepahi, A.A. (2011) Petrology and Geochemistry of Aligoodarz Granitoid, Western Iran: Implications for Petrogenetic Relation with Boroujerd and Dehno Granitoids. *Geopersia*, **1**, 67-86.

[71] Marchand, P. (2005) Caractérisation de deux intrusions kimberlitiques au témiscamingue, notre-dame-du-nord 1 et belleterre (bt 44) et de deux dykes ultra-mafiques des monts Torngat. Université Laval.

[72] Chappell, B.V. and White, A.J.R. (1974) Two Contrasting Granite Types. *Pacific Geology*, **8**, 173-174.

[73] Sisson, T.W., Ratajeski, K., Hankins, W.B. and Glazner, A.F. (2004) Voluminous Granitic Magmas from Common Basaltic Sources. *Contributions to Mineralogy and Petrology*, **148**, 635-661. https://doi.org/10.1007/s00410-004-0632-9

[74] Xu, H., Ma, C., Zhao, J. and Zhang, J. (2014) Magma Mixing Generated Triassic I-Type Granites in South China. *The Journal of Geology*, **122**, 329-351. https://doi.org/10.1086/675667

[75] Taylor, S.R. and McLennan, S.M. (1985) The Continental Crust: Its Composition and Evolution. Blackwell Scientific, Oxford. Cambridge University Press.

[76] Rollinson, H.R. (1993) Using Geochemical Data: Evaluation, Presentation, Interpretation, Geochemistry Series. John Wiley & Sons.

[77] Glodji, L.A. (2012) La zone de cisaillement de Kandi et le magmatisme associé dans la région de Savalou-Dassa (Bénin): Étude structurale, pétrologique et géochronologique. Master's Thesis, Universités Jean Monnet Saint-Etienne et d'AbomeyCalavi.

[78] Jochum, K.P., McDonough, W.F., Palme, H. and Spettel, B. (1989) Compositional Constraints on the Continental Lithospheric Mantle from Trace Elements in Spinel Peridotite Xenoliths. *Nature*, **340**, 548-550. https://doi.org/10.1038/340548a0

[79] Abdel-Rahman, A.M. and Nassar, P.E. (2004) Cenozoic Volcanism in the Middle East: Petrogenesis of Alkali Basalts from Northern Lebanon. *Geological Magazine*, **141**, 545-563. https://doi.org/10.1017/s0016756804009604

[80] Dupuis, C. (2005) Pétrologie et géochimie des provinces mésozoïques téthysiennes reliées à lazone de suture Yarlung-Zangbo, Tibet. Ph.D. Thesis, Université Laval.

[81] Hoffer, G. (2008) Fusion partielle d'un manteau métasomatisé par un liquide adakitique: Approches géochimique et expérimentale de la genèse et de l'évolution des magmas de l'arrière-arc équatorien. Master's Thesis, Blaise Pascal University.

[82] Müller, D., Groves, D.I. (2000). Potassic Igneous Rocks and Associated Gold-Copper Mineralization, Mineral Resource Reviews. Springer. https://doi.org/10.1007/978-3-319-23051-1

[83] Harris, N.B.W., Pearce, J.A. and Tindle, A.G. (1986) Geochemical Characteristics of Collision-Zone Magmatism. *Geological Society*, *London*, *Special Publications*, **19**, 67-81. https://doi.org/10.1144/gsl.sp.1986.019.01.04

[84] Pearce, J.A., Harris, N.B.W. and Tindle, A.G. (1984) Trace Element Discrimination Diagrams for the Tectonic Interpretation of Granitic Rocks. *Journal of Petrology*, **25**, 956-983. https://doi.org/10.1093/petrology/25.4.956